

Electron-Transfer Mechanism for Aromatic Nitration via the Photoactivation of EDA Complexes. Direct Relationship to Electrophilic Aromatic Substitution

E. K. Kim, T. M. Bockman, and J. K. Kochi*

Contribution from the Chemistry Department, University of Houston, Houston, Texas 77204-5641

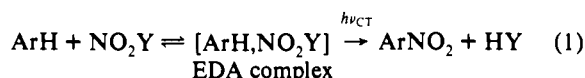
Received November 20, 1992

Abstract: Charge-transfer nitration of various aromatic hydrocarbons (ArH) is readily achieved by the deliberate photoactivation of their electron donor-acceptor (EDA) complexes with *N*-nitropyridinium (PyNO₂⁺). Time-resolved spectroscopy unambiguously identifies (ArH⁺, NO₂, Py) as the reactive triad resulting directly from the charge-transfer activation of the [ArH,PyNO₂⁺] complex; and the subsequent homolytic annihilation of the aromatic cation radical with NO₂ leads to the Wheland intermediate pertinent to aromatic nitration. Charge-transfer nitration of such aromatic donors as toluene, anisole, mesitylene, and *tert*-butylbenzene as well as the polymethylbenzenes and substituted anisoles forms the basis for detailed comparisons with the products from electrophilic aromatic nitration, especially with regard to the unique isomer distributions, nuclear versus side-chain nitrations, and ipso adducts in nonconventional nitrations. Mechanistic implications are discussed in terms of the electron-transfer activation of electrophilic aromatic nitration.

Introduction

Electrophilic aromatic nitrations that are commonly carried out with nitric acid¹ and other nitronium "carriers" (NO₂Y) such as acetyl nitrate, dinitrogen pentoxide, nitryl chloride, *N*-nitropyridinium, tetranitromethane, etc.² involve the spontaneous formation of preequilibrium amounts of precursor complexes.³ These transitory intermediates are generally ignored from further consideration,⁴ although they are unambiguously identified by their characteristic charge-transfer absorption bands ($h\nu_{CT}$),⁸⁻¹⁰ which are uniformly red-shifted by decreasing ionization potentials of the aromatic hydrocarbon (ArH) and by increasing electron affinities of NO₂Y acting as electron donors and electron acceptors, respectively, in Mulliken's terminology.^{11,12}

Directly relevant to aromatic nitration are the nitroarenes ArNO₂ obtainable by the alternative *photochemical* activation (via the charge-transfer bands, $h\nu_{CT}$) of such electron donor-acceptor or EDA complexes, i.e.



with NO₂Y being either tetranitromethane¹³ or *N*-nitropyridin-

ium.¹⁴ The latter is particularly noteworthy since the more common electrophilic activity of the *N*-nitropyridinium cation as a *thermal* nitrating agent has been shown to be strongly modulated by substituents on the heteroaromatic moiety.¹⁵⁻¹⁷ Since the photochemical and electrophilic aromatic nitrations with *N*-nitropyridinium are carried out under essentially the same experimental conditions—the charge-transfer activation being merely effected with light at lower temperatures where competition from the thermal process is unimportant—any mechanistic insight obtained about the photochemical nitration will bear directly on the mechanism of electrophilic aromatic nitration.¹⁸ We have accordingly focussed on the photochemical nitration of selected aromatic (benzenoid) donors for which widely varying isomeric compositions and distinctive products have been previously identified in electrophilic nitrations.¹⁹⁻²¹ Specifically, in this study are included the nitration of (a) anisole for the different ratios of *o/p*-nitroanisole,^{22,23} (b) toluene for ortho/para versus meta nitration,²⁴ (c) polymethylbenzene (especially durene) for nuclear versus side-chain nitration²⁵⁻²⁷ and the formation of aromatic

(14) Sankararaman, S.; Kochi, J. K. *J. Chem. Soc., Perkin Trans. 2* **1991**, 1.

(15) Olah, G. A.; Olah, J. A.; Overchuk, N. A. *J. Org. Chem.* **1965**, *30*, 3373. Olah, G. A.; Narang, S. C.; Olah, J. A.; Pearson, R. L.; Cupas, C. A. *J. Am. Chem. Soc.* **1980**, *102*, 3507.

(16) Kim, E. K.; Lee, K. Y.; Kochi, J. K. *J. Am. Chem. Soc.* **1992**, *114*, 1756.

(17) Kim, E. K.; Bockman, T. M.; Kochi, J. K. *J. Chem. Soc., Perkin Trans. 2* **1992**, 1879.

(18) Kochi, J. K. *Acc. Chem. Res.* **1992**, *25*, 39.

(19) (a) Stock, L. M. *Prog. Phys. Org. Chem.* **1976**, *12*, 21. (b) Taylor, R. *Electrophilic Aromatic Substitution*; Elsevier: New York, 1991.

(20) Suzuki, H. *Synthesis* **1977**, 217.

(21) Hartshorn, S. R. *Chem. Soc. Rev.* **1974**, *3*, 167.

(22) Barnett, J. W.; Moodie, R. B.; Schofield, K.; Weston, J. R.; Coombes, R. G.; Golding, J. G.; Tobin, G. D. *J. Chem. Soc. Perkin Trans. 2*, **1977**, 248.

(23) (a) Norman, R. O. C.; Radda, G. K. *J. Chem. Soc.* **1961**, 3030. (b) Hartshorn, S. R.; Schofield, K. *Prog. Org. Chem.* **1973**, *8*, 298.

(24) (a) Olah, G. A.; Malhotra, R.; Narang, S. C. in ref 2, see Table 41, p 150ff. See, also: (b) Coon, C. L.; Blucher, W. G.; Hill, M. E. *J. Org. Chem.* **1973**, *38*, 4243. (c) Duffy, J. L.; Laali, K. K. *J. Org. Chem.* **1991**, *56*, 3006.

(d) Olah, G. A.; Krishnamurthy, V. V.; Narang, S. C. *J. Org. Chem.* **1982**, *47*, 596. (e) Masci, B. J. *Org. Chem.* **1985**, *50*, 4081.

(25) Blackstock, D. J.; Fischer, A.; Richards, K. E.; Wright, G. J. *Aust. J. Chem.* **1973**, *26*, 775.

(26) (a) Suzuki, H.; Koide, H.; Taki, Y.; Ohbayashi, E.; Ogawa, T. *Chem. Lett.* **1987**, 891. (b) Ebersson, L.; Nyberg, K. *Tetrahedron Lett.* **1966**, 2389.

(27) Masnovi, J. M.; Sankararaman, S.; Kochi, J. K. *J. Am. Chem. Soc.* **1989**, *111*, 2263.

(1) Schofield, K. *Aromatic Nitration*; Cambridge University Press: New York, 1980.

(2) Olah, G. A.; Malhotra, R.; Narang, S. C. *Nitration. Methods and Mechanisms*; VCH: New York, 1989.

(3) Kochi, J. K. *Pure Appl. Chem.* **1991**, *63*, 255.

(4) The exception is the parent electrophile NO₂⁺, for which π -complex formation has been delineated in solution⁵ and in the gas phase.^{6,7}

(5) Olah, G. A.; Kuhn, S. J.; Flood, S. H. *J. Am. Chem. Soc.* **1961**, *83*, 4571. For a review, see Olah et al. in ref 2.

(6) Schmitt, R. J.; Buttrill, S. E., Jr.; Ross, D. S. *J. Am. Chem. Soc.* **1981**, *103*, 5265; **1984**, *106*, 926. See, also: Attina, M.; Cacace, F.; Yanez, M. *J. Am. Chem. Soc.* **1987**, *109*, 5092.

(7) Compare, also: Reents, W. D., Jr.; Freiser, B. S. *J. Am. Chem. Soc.* **1980**, *102*, 271.

(8) Masnovi, J. M.; Hilinski, E. F.; Rentzepis, P. M.; Kochi, J. K. *J. Am. Chem. Soc.* **1986**, *108*, 1126.

(9) Foster, R. *Organic Charge-Transfer Complexes*; Academic: New York, 1969.


(10) Andrews, L. J.; Keefer, R. M. *Molecular Complexes in Organic Chemistry*; Holden-Day: San Francisco, 1964.

(11) Mulliken, R. S. *J. Am. Chem. Soc.* **1952**, *74*, 811.

(12) Mulliken, R. S.; Person, W. B. *Molecular Complexes. A Lecture and Reprint Volume*; Wiley: New York, 1969.

(13) Sankararaman, S.; Haney, W. A.; Kochi, J. K. *J. Am. Chem. Soc.* **1987**, *109*, 5235, 7824.

Table I. Charge-Transfer Absorption of Aromatic EDA Complexes with *N*-Nitropyridinium^a

aromatic donor	M	IP, ^b eV	λ_{exc} , ^c nm	X— 			λ_{CT} , ^d nm	<i>T</i> , ^e °C
				X	M	nm ^c		
benzene	0.8	9.23	280	MeO	0.08	350	<350	
benzene	0.02	9.23	280	MeO ₂ C	0.23	360	385	
chlorobenzene	0.06	9.07	300	MeO ₂ C	0.03	350		-40
toluene	0.09	8.82	300	MeO ₂ C	0.04	340		-40
toluene	0.9	8.82	300	H	0.08	340	340	-20
anisole	0.08	8.39	340	MeO	0.08	350	400	
anisole	0.09	8.39	340	MeO ₂ C	0.08	340	475 (410)	-40
<i>p</i> -xylene	0.6	8.44	300	MeO	0.05	350	365	
	0.3		300	MeO ₂ C	0.03	340	438	
biphenyl	0.2	8.45	320	H	0.2	340	400	
4-chloroanisole	0.05	8.4 ^f	310	H	0.05	340	420	
4-bromoanisole	0.1	8.3 ^f	310	H	0.05	340	410	
4-methylanisole	0.1	8.18	310	H	0.08	340	450 (380)	-20
mesitylene	0.2	8.42	310	MeO	0.09	350	380 (330)	
mesitylene	0.2	8.42	310	MeO ₂ C	0.03	340	435 (360)	
durene	0.4	8.05	300	MeO	0.04	350	390 (341)	
durene	0.06	8.05	300	MeO ₂ C	0.03	340		-40
pentamethylbenzene	0.3	7.92	300	MeO	0.03	350	480 (351)	
	0.08		300	MeO ₂ C	0.04	340	(440)	-40
hexamethylbenzene	0.04	7.85	310	MeO	0.05	350	520 (382)	

^a In acetonitrile at the concentrations of ArH and XPyNO₂⁺ indicated. ^b Ionization potential from ref 32. ^c Low-energy cutoff (*A* < 0.05). ^d Wavelength at which the extinction coefficient of the CT band attains a value of 50 M⁻¹ cm⁻¹ (CT band maximum in parenthesis). ^e Temperature 23 °C, unless indicated otherwise. ^f Estimated from the data in ref 13.

dimers,²⁸ and (d) *tert*-butylbenzene, bromoanisole, and methylanisole for transalkylation,²⁹ bromine transfer,^{13,30} and demethylation,³¹ respectively, via ipso addition. Such product comparisons are augmented by mechanistic studies involving time-resolved (UV-vis) spectroscopy to identify the reactive intermediates in the photochemical nitration and to follow their temporal decay as they evolve to the various nitroarenes.

Results

I. Charge-Transfer Absorptions of Aromatic EDA Complexes with *N*-Nitropyridinium. When a colorless solution of *N*-nitro-4-carbomethoxy-pyridinium in acetonitrile was mixed with anisole at -40 °C, it immediately turned orange; and similarly, the addition of toluene spontaneously led to a bright yellow solution. The quantitative effects of such color changes were apparent in the electronic (UV-vis) spectra by the appearance of the new absorptions shown in Figure 1. The progressive bathochromic shift with the decreasing values of the ionization potentials (IP) of the aromatic donors,³² as presented in Table I,³³ accords with the spectral assignment of the new absorptions to charge-transfer transitions.^{9,12}

The spectrophotometric analysis of the absorbance changes accompanying the variations in the ArH concentrations was carried out by the Benesi-Hildebrand method^{35,36} to yield representative values of the formation constants $K_{\text{EDA}} \sim 0.6 \text{ M}^{-1}$

(28) (a) Bewick, A.; Edwards, G. J.; Mellor, J. M. *Tetrahedron Lett.* **1975**, 4685. (b) Lau, W.; Kochi, J. K. *J. Am. Chem. Soc.* **1984**, *106*, 7100.

(29) (a) Olah, G. A.; Kuhn, S. J. *J. Am. Chem. Soc.* **1964**, *86*, 1067. (b) Myhre, P. C.; Beug, M. *J. Am. Chem. Soc.* **1966**, *88*, 1568, 1569. See, also: Kim et al. in ref 16.

(30) (a) Perrin, C. L.; Skinner, G. A. *J. Am. Chem. Soc.* **1971**, *93*, 3389. (b) Clewly, R. G.; Fischer, A.; Henderson, G. N. *Can. J. Chem.* **1989**, *67*, 1472.

(31) (a) Barnes, C. E.; Myhre, P. C. *J. Am. Chem. Soc.* **1978**, *100*, 973. (b) Fischer, A.; Henderson, G. N.; RayMahasay, S. *Can. J. Chem.* **1987**, *65*, 1233.

(32) (a) Howell, J. O.; Goncalves, J. M.; Amatore, C.; Klasinc, L.; Wightman, R. M.; Kochi, J. K. *J. Am. Chem. Soc.* **1984**, *106*, 3968. (b) *p*-Chloro- and *p*-bromoanisole estimated from (a) above and ref 13.

(33) Owing to the obscuration of the CT band maximum in some EDA complexes by the low-energy tail absorption of the *N*-nitropyridinium (e.g., see toluene in Figure 1), the value of λ_{CT} , the wavelength at which the CT extinction coefficient is equal to 50 M⁻¹ cm⁻¹, was used as a uniform measure (see supplementary material).³⁴

(34) Compare, also: Tsubomura, H.; Mulliken, R. S. *J. Am. Chem. Soc.* **1960**, *82*, 5966.

(35) Benesi, H. A.; Hildebrand, J. H. *J. Am. Chem. Soc.* **1949**, *71*, 2703.

(36) Person, W. B. *J. Am. Chem. Soc.* **1965**, *87*, 167.

for the 1:1 EDA complexes, i.e.

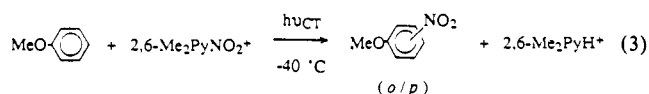


as exemplified by the nitrating agent MeOPyNO₂⁺ and either pentamethylbenzene or 9-methylanthracene.¹⁶

The charge-transfer absorption bands described above were transient, but they persisted unchanged for prolonged periods when the temperature of the solution was simply lowered to retard the electrophilic process(es). The deliberate irradiation at this (low) temperature with the focussed output of a 500-W mercury lamp equipped with a sharp cutoff filter (Corning CS series) effectively promoted the photochemical transformations which are hereafter designated as *charge-transfer nitrations*. For each aromatic donor, the appropriate cutoff filter was carefully chosen (Table I) to remove all extraneous light so as to ensure the selective excitation of only the charge-transfer absorption band (compare Figure 1). Under these controlled conditions, there could be no ambiguity about the adventitious excitation of either the uncomplexed arene or the nitrating agent.

II. Charge-Transfer Nitration of Aromatic Donors by the Direct Irradiation of EDA Complexes with *N*-Nitropyridinium. The charge-transfer nitrations of the following aromatic donors were generally carried out to rather low actinic conversions to avoid complications from light absorption by the nitroarene products and in duplicate sets (with a dark control) to simultaneously monitor any competition from thermal processes.

Anisole. The yellow solution of anisole and Me₂PyNO₂⁺ in acetonitrile at -40 °C was irradiated with the aid of the cutoff filter CS-3391 that effectively removed all excitation light with $\lambda_{\text{exc}} < 400 \text{ nm}$ (see Experimental Section). The periodic ¹H NMR analysis of the clear pale photolysate indicated the presence of lutidinium and a mixture of *o*- and *p*-nitroanisole. After reasonable photochemical conversions were attained (Table II), the ¹H NMR spectrum was found to be virtually identical to that of the reaction mixture obtained by electrophilic (thermal) nitration, as also shown by the quantitative comparison of the products in entries 1 and 2 (Table II).



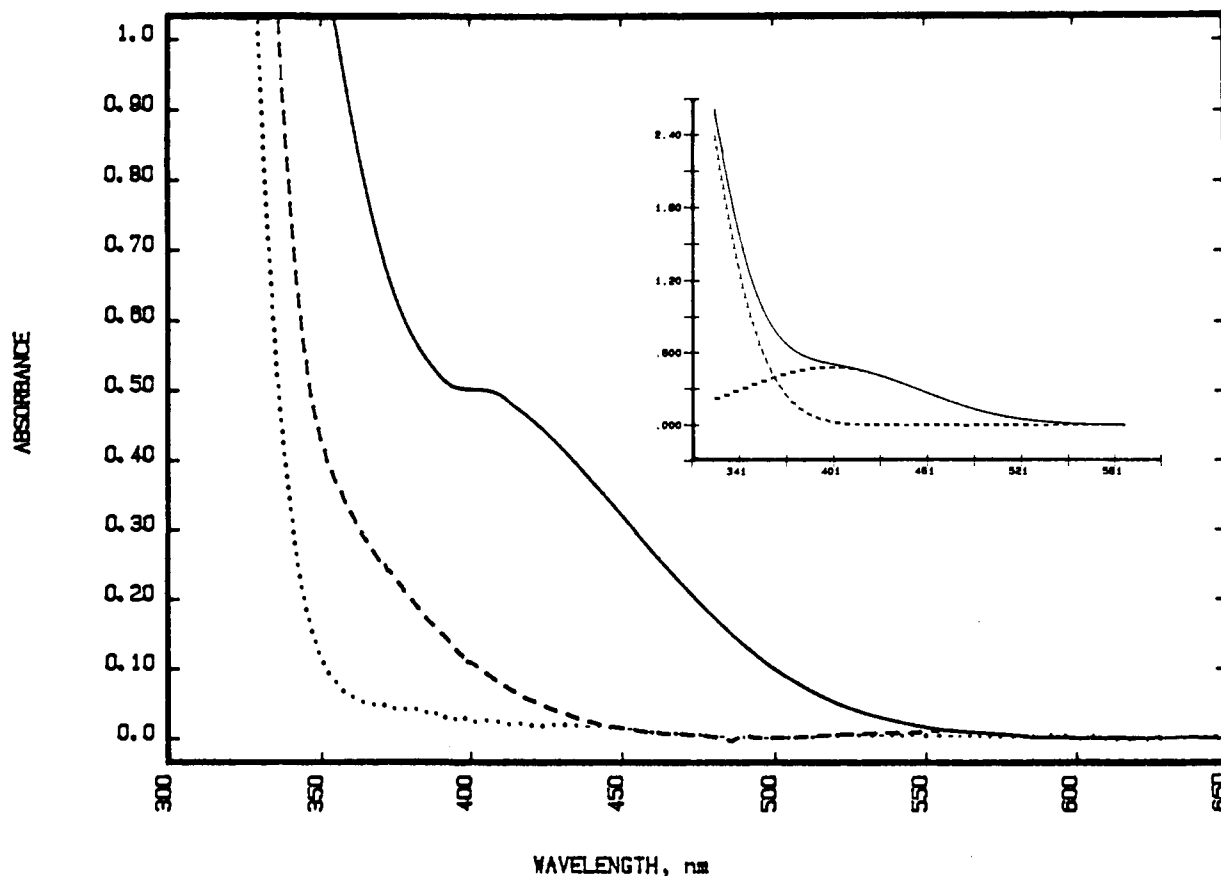


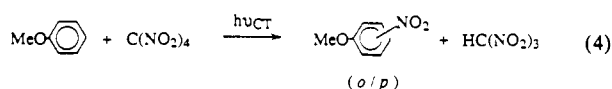
Figure 1. Typical charge-transfer spectra of the aromatic donors anisole (—) and toluene (---) with $\text{MeO}_2\text{CPyNO}_2^+$ in acetonitrile at -40°C . Spectrum of the acceptor alone (···). The inset shows the Gaussian (digital) deconvolution for the CT band of the anisole EDA complex with $\lambda_{\text{CT}} = 410\text{ nm}$.

Table II. Charge-Transfer Nitration of Anisole with X-Substituted *N*-Nitropyridinium Cations^a

X	μmol	anisole, μmol	$\lambda_{\text{exc}},^b$ nm	nitroanisole ^c %		conv, ^d %	temp/time $^\circ\text{C}/\text{h}$
				<i>o</i>	<i>p</i>		
2,6-Me ₂	60	184	400	65	35	47	-40/35
4-MeO	120	60	dark	69	31	30	60/21
4-MeO ₂ C	90	180	400	71	29	8	-40/24
H	100	280	350 ^e	51	49	4	-30/6
4-Me	190	380	350 ^e	51	49	18	10/9.5
4-MeO	80	180	350 ^e	41	56 ^f	9	-40/7.5
4-MeO	90	280	350 ^e	37	63	10	23/6.5
4-MeO	145 ^g	156	410	40	60	3	23/2.5
4-MeO	100 ^h	180	380	38	62 ⁱ	13	23/2
$\text{C}(\text{NO}_2)_4$ ^j			425	43	53 ^k		

^a In acetonitrile, unless indicated otherwise. ^b High-energy cutoff of Pyrex filter. ^c Isomer distribution with *m* too low to detect (<1%), unless indicated otherwise. ^d Conversion based on anisole recovered. ^e Broad-band (350–580 nm) filter. ^f Also ~3% meta isomer. ^g In benzene solution. ^h With 5% vol of added trifluoroacetic acid. ⁱ Includes ~20% unidentified product. ^j From ref 13. ^k Also 4% meta isomer.

In order to examine the effect of the nitrating agent, anisole was treated with $\text{MeO}_2\text{CPyNO}_2^+$, PyNO_2^+ , and MeOPyNO_2^+ *seriatim* under the conditions listed in Table II. This also includes the parallel nitration of anisole with the tetranitromethane (TNM) acceptor, i.e.



for which the charge-transfer nitration has been previously delineated.¹³

Toluene. The charge-transfer nitration of toluene with 2,6-Me₂PyNO₂⁺ was carried out at -40°C (to low conversions with $\lambda_{\text{exc}} > 410\text{ nm}$) to afford a nitrotoluene mixture consisting

Table III. Effects of the Nitrating Agent on the Charge-Transfer Nitration of Toluene^a

X	μmol	toluene, μmol	$\lambda_{\text{exc}},^b$ nm	nitrotoluene, ^c %			yield, ^d %	temp/time $^\circ\text{C}/\text{h}$
				<i>o</i>	<i>m</i>	<i>p</i>		
2,6-Me ₂	120	1410	410	70	~2	28	4.4	-40/16
4-MeO ₂ C	74	190	350 ^e	28	42	30	3.3	-40/16
H	160	1900	380	24	60	16	2.7	-20/1
4-Me	100	280	350 ^e	23	54	23	8.3	23/21
4-MeO	140	350	350 ^e	14	59	27	11	23/42
4-MeO	100 ^f	180	350 ^e	20	43	37	3.3	-65/40
4-MeO	210 ^g	480	380	28	52	20	1	23/3.3
4-MeO	100 ^h	94	380	46	17	28	3.4	23/18
4-MeO	95 ⁱ	370	380	60	17	23	41 ^j	23/17
4-MeO	95 ⁱ	190	380	66	5	28	2 ^k	-40/17
Tetranitromethane								
$\text{C}(\text{NO}_2)_4$	210	245	400	28	32	40	3.3	-40/70
$\text{C}(\text{NO}_2)_4$	170	240	400	26	32	42	2.6	23/13
$\text{C}(\text{NO}_2)_4$	210 ^g	480	410	32	31	37	2.8	23/15

^a In acetonitrile, unless indicated otherwise. ^b High-energy cutoff of Pyrex filter. ^c Isomer distribution. ^d Total yield of $\text{CH}_3\text{C}_6\text{H}_4\text{NO}_2$ based on the minor reactant. ^e Broad-band (350–580 nm) filter. ^f In *n*-butyronitrile solvent. ^g With 5% vol added trifluoroacetic acid. ^h Dichloromethane solvent. ⁱ With ~20-fold excess of added dinitrogen tetroxide. ^j Plus benzaldehyde (~20%) and α -nitrotoluene (~15%). ^k Plus benzaldehyde (~50%).

primarily of ortho/para isomers in a ratio (Table III) that was essentially indistinguishable from that previously obtained in electrophilic (thermal) nitration.¹⁶ However, a substantial increase in the meta isomer was apparent when the charge-transfer nitration of toluene was effected with $\text{MeO}_2\text{CPyNO}_2^+$, PyNO_2^+ , and MeOPyNO_2^+ in entries 2, 3, and 5 as well as tetranitromethane (entries 11 and 12). In order to trace the origin of such an (unusual) isomer distribution, the CT nitration of toluene was further examined with MeOPyNO_2^+ at different temperatures in other solvents, and in the presence of added trifluoroacetic acid (TFA). Interestingly, the latter effectively reduced the

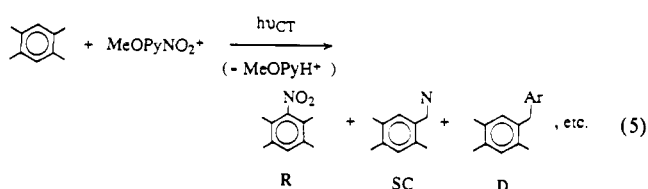
Table IV. Side-Chain Nitration and Oxidative Dimer Formation in the Charge-Transfer Nitration of Various Polymethylbenzenes^a

aromatic donor ^b	XPyNO ₂ ⁺ X	λ _{exc.} , nm	products, ^c %			conv. %	temp/time °C/h
			R	SC	D		
DUR	4-MeO	415	8	90	2	80	23/16
DUR	4-MeO	400	2	81	17	49	-30/16
DUR ^d	4-MeO	410	21	77 ^e	3	80	23/5
DUR	4-Me	400	7	87	6	40	0/16
DUR	H	425	13	73	14	30	-20/3
DUR ^f	TNM	425	21	77	2		23/
PMB	4-MeO ₂ C	400	10	40	50	32	-40/5
PMB	H	400	7	52	41	24	-40/5
XYL	4-MeO	380	65	37 ^g	h	45	23/20
MES	2,6-Me ₂	410	100	h	h	53	-40/18
MES	4-MeO	410	100 ⁱ	h	h	24	23/20
MES ^d	4-MeO	380	100 ^j	h	h	30	30/27
MES	4-Me	380	100 ^k	h	h	75	0/13
HMB	4-MeO	400	0	100	0	66	23/10
HMB	H	415	0	100	0	50	-5/5

^a In acetonitrile, as in Tables II and III. ^b Durene = DUR, pentamethylbenzene = PMB, *p*-xylene = XYL, hexamethylbenzene = HMB, and mesitylene = MES. ^c Molar distribution of products from ring nitration, side-chain substitution, and dimer formation, as described in the text. ^d With 5% vol added trifluoroacetic acid. ^e Includes 2,4,5-trimethylbenzyl trifluoroacetate (50%). ^f From ref 27. ^g Includes 22% side-chain nitrate. ^h Below detection limit (<1%). ^{i-k} Includes 75% (i), 66% (j), or 77% (k) of corresponding ring pyridination (see Experimental Section).

isomeric meta content in charge-transfer nitration carried out in dichloromethane (entry 8) but it was ineffective in acetonitrile (entry 7). It is important to note that excess NO₂ (added as dinitrogen tetroxide in entry 9) led to the significant reduction of *m*-nitrotoluene, so that at low temperatures the isomeric distribution closely approached that¹⁶ obtained in electrophilic nitration (see entry 10, Table III).

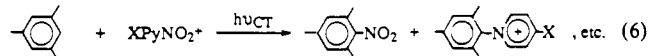
Durene and Other Polymethylbenzenes. The charge-transfer nitration of durene could be examined over a (50-degree) temperature range with MeOPyNO₂⁺ owing to its significantly lower electrophilic reactivity. The subsequent ¹H NMR and HPLC analysis of the photolysate (see Experimental Section) indicated the presence of the expected ring-nitrated R together with the side-chain-substitution product(s) SC and the dimeric diphenylmethane D according to the stoichiometry in Table IV, i.e.



where N = nitro, nitrito, acetamido, etc. and Ar = 2,3,5,6-tetramethylphenyl.¹⁶ The same CT irradiation at the lower temperature of -30 °C led to substantially greater yields of D, largely at the expense of ring nitration (see entry 2, Table IV). A similar enhancement of D was observed when MeOPyNO₂⁺ was replaced by PyNO₂⁺, but at the expense of the side-chain substitution (entry 5). On the other hand, the presence of added trifluoroacetic acid had the opposite effect—increasing ring nitration at the expense of dimer formation (entry 3). The formation of oxidative dimers D generally paralleled the number of methyl groups on the aromatic donor. Thus it constituted an important process in the charge-transfer nitration of pentamethylbenzene that was accompanied by a concomitant decrease in side-chain nitration, as listed in Table IV, entries 7 and 8. Moreover, this trend in dimer yields extended to *p*-xylene, for which no dimeric trimethyldiphenylmethane, and only minor amounts of side-chain-substitution products, were observed.

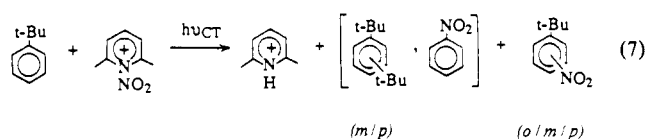
Hexamethylbenzene and mesitylene represented the extremes of polymethylbenzene behavior in Table IV, and charge-transfer nitration led to only side-chain nitration (entries 14 and 15) and

ring substitution (entries 10–13), respectively. Particularly noteworthy in the latter regard was the quantitative conversion of mesitylene with the sterically hindered Me₂PyNO₂⁺ to nitromesitylene (entry 10). However, there was significantly competition from the unique ring pyridination of mesitylene, i.e.



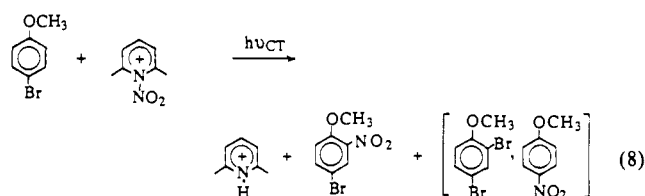
when X = CH₃O and CH₃ (Table IV, entries 11 and 13), which was diminished (but not completely eliminated) by the presence of added trifluoroacetic acid (entry 12).

***tert*-Butylbenzene, 4-Bromo-, and 4-Methylanisole.** *Trans*-alkylation accompanied the charge-transfer nitration of *tert*-butylbenzene with Me₂PyNO₂⁺ at -40 °C, as indicated in Table V by the formation of di-*tert*-butylbenzene (and nitrobenzene), in addition to *o*-, *m*-, and *p*-nitro-*tert*-butylbenzene with essentially the same isomeric distribution obtained in electrophilic nitration,¹⁶ i.e.



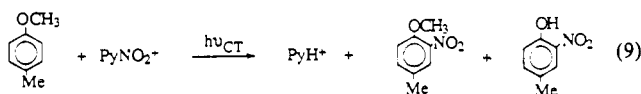
Although ipso substitution of *tert*-butylbenzene also occurred with MeOPyNO₂⁺, PyNO₂⁺, and MeO₂CPyNO₂⁺, as indicated in entries 2, 7, and 8 by the substantial amounts of di-*tert*-butylbenzene and nitrobenzene observed, the meta content of the nitro-*tert*-butylbenzene fraction was significantly enhanced (similar to that observed with toluene in Table III). However, it is noteworthy that the charge-transfer nitration of *tert*-butylbenzene with MeOPyNO₂⁺ in the presence of either excess NO₂ (entry 5) or trifluoroacetic acid (entry 4) led to the restoration of the electrophilic pattern of isomeric product distribution.

*Trans*halogenation accompanied the charge-transfer nitration of *p*-bromoanisole with either Me₂PyNO₂⁺ or PyNO₂⁺ at -40 °C, as indicated in Table V (entries 9 and 10) by the concomitant formation of nitroanisole and dibromoanisole (together with small amounts of tribromoanisole), in addition to the expected product of ring nitration,¹³ i.e.



Moreover, the same product distribution obtained in the electrophilic nitration of 4-bromoanisole with Me₂PyNO₂⁺ carried out (in the dark) at 23 °C. A small but discrete amount of *p*-dibromobenzene (and nitrobenzene) accompanied the charge-transfer nitration of bromobenzene to *m*- and *p*-nitrobromobenzene at either 23 or -40 °C. However, no *trans*halogenation was observed in the charge-transfer nitration of either 4-chloroanisole or chlorobenzene.

*Trans*methylation was observed in the charge-transfer nitration of *p*-methylanisole with PyNO₂⁺ at -20 °C by the formation of substantial amounts of *o*-nitro-*p*-cresol that were obtained in addition to ring nitration,¹³ i.e.



Furthermore, small amounts of the isomeric 4-nitro-4-methylcyclohexa-2,5-dienone³⁷ were detected. Control experiments

Table V. Ipso Substitution in the Charge-Transfer Nitration of *tert*-Butylbenzene, 4-Bromo-, and 4-Methylanisole^a

ArH	XPyNO ₂ ⁺ X	λ _{exc} , nm	product distribution ^b		conv. %	temp/time °C/h
			ArNO ₂ % (o/m/p)	ipso % (%)		
<i>tert</i> -butylbenzene	2,6-Me ₂	380	97 (6/12/82)	2 (1)	44	-40/42
	4-MeO	350 ^c	45 (5/73/22)	40 (15)	23	23/18
	4-MeO	350 ^c	70 (4/75/21)	20 (10)	11	-40/45
	4-MeO ^c	350 ^c	80 (7/15/78)	17 (3)	4	23/45
	4-MeO ^d	380	98 (16/22/62)	2 (-)	19	23/20
	4-Me	350 ^c	77 (4/64/32)	16 (7)	9	23/17
	H	350 ^c	66 (6/71/23)	27 (7)	5	-20/9
	4-MeO ₂ C	350 ^c	50 (0/57/43)	40 (10)	7	-40/12
	4-bromoanisole	2,6-Me ₂	380	50 ⁱ	30 ^j (20)	63
H		410	45 ⁱ	20 ^j (25)	63	-40/4
4-methylanisole	H	425	65 ^j	35 ^k	25	-20/3.5
	4-MeO	350 ^c	40 (0/60/40)	h (2)	4	23/48
bromobenzene	4-MeO	350 ^c	30 (0/81/19)	h (2)	9	-40/41

^a In acetonitrile, as in Tables II and III. ^b For ArNO₂, combined yield (isomer distribution). For ipso substitution: *tert*-butylbenzene, 1,3- and 1,4-di-*tert*-butylbenzene (nitrobenzene); 4-bromoanisole, 2,4-dibromoanisole (4-nitroanisole); 4-methylanisole, *o*-nitro-*p*-cresol; bromobenzene, 1,2- and 1,4-dibromobenzene (nitrobenzene). ^c With 50% vol added trifluoroacetic acid in dichloromethane. ^d With excess dinitrogen tetroxide. ^e Broad-band filter. ^f Includes 2,4,6-tribromoanisole and anisole. ^g Includes 4-nitro-4-methylcyclohexa-2,5-dienone. ^h 1,2- And 1,4-dibromobenzene. ⁱ 2-Nitro-4-bromoanisole. ^j 2-Nitro-4-methylanisole.

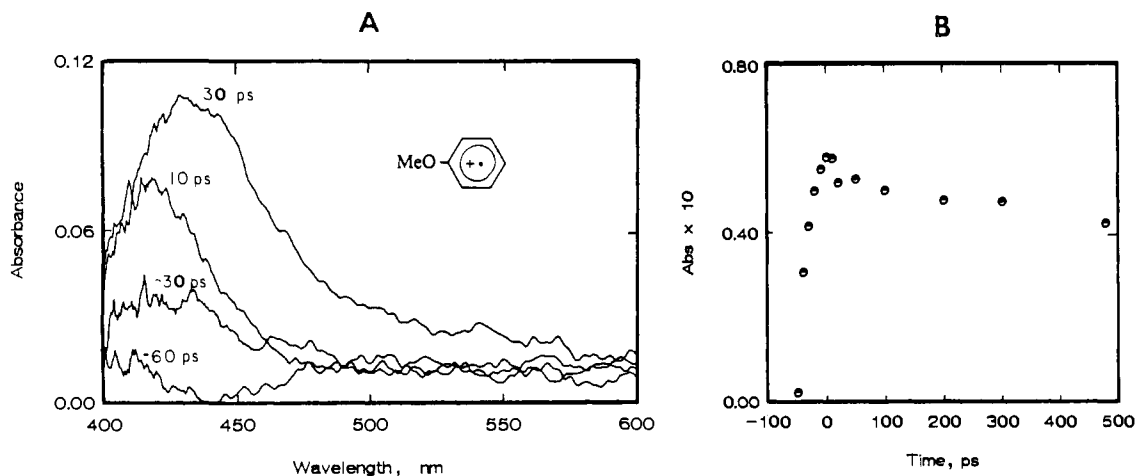


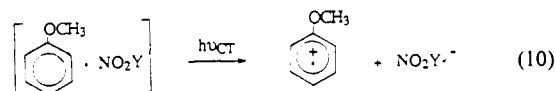
Figure 2. (A) Time-resolved (picosecond) spectra of anisole cation radical following the 355-nm excitation of the EDA complex from 0.4 M anisole and 0.04 M MeOPyNO₂⁺ in acetonitrile at the measurement times indicated. (B) Temporal evolution of the absorbance at λ_{mon} = 435 nm.

established that neither *p*-methylanisole nor the *o*-nitroanisole product was demethylated under conditions of the charge-transfer nitration.

III. Time-Resolved (Picosecond) Spectroscopy of Aromatic Cation Radicals as the Reactive Intermediates in Charge-Transfer Nitration. To identify the reactive intermediates responsible for charge-transfer nitration, we initially examined the time-resolved spectra of the transients following the application of a 30-ps (fwhm) laser pulse. The third harmonic at 355 nm of the mode-locked Nd³⁺:YAG laser was used to excite the charge-transfer band. The typical CT absorption spectra in Figure 1 and the spectral data in Table I indicated that λ_{exc} = 355 nm would specifically excite only the aromatic EDA complex with nitropyridinium, and it could not lead to the local-band excitation¹² of either the free (uncomplexed) aromatic donor³⁸ or the cationic acceptor.¹⁶ Owing to the generally high yields of nitration products obtained in Tables II–IV, the laser-pulse excitation of the charge-transfer bands was examined with the following four prototypical aromatic donors.

Anisole. Upon the 355-nm irradiation of the EDA complex from anisole (AN) and the *N*-nitro-4-methoxypyridinium acceptor in acetonitrile (under the conditions of the CT nitration in eq 3), an intense, broad absorption band was observed immediately. Thus Figure 2 shows the growth of the new absorption within the bandwidth (30-ps, fwhm) of the laser pulse.³⁹ The position (λ_{max} = 435 nm) and bandshape (fwhm) of the new transient at *t* = 30 ps coincided with the absorption spectrum of the cation radical of anisole (AN^{•+}) generated previously by pulse radiolysis.^{40,41}

Parallel time-resolved spectroscopic studies were also carried out for the charge-transfer excitation of the anisole complex with tetranitromethane (TNM) pertinent to the photochemical nitration in eq 4. Owing to the residual TNM absorbance at 355 nm,⁸ the second harmonic at 532 nm of the Nd³⁺:YAG laser was used to excite the low-energy tail of the CT absorbance. Notably, the transient spectra were identical to those from the photoexcitation of the anisole EDA complex with MeOPyNO₂⁺ in Figure 2A, i.e.



where NO₂Y = MeOPyNO₂⁺ or C(NO₂)₄. Moreover, the same spectrum of AN^{•+} was produced by the photoinduced electron transfer from anisole via the triplet sensitization and quenching of benzophenone, as described in the Experimental Section.

The temporal evolution of the anisole cation radical attendant upon the CT excitation of the [AN, MeOPyNO₂⁺] complex was followed by the continual monitoring of its absorbance change at λ_{mon} = 435 nm. Thus Figure 2B shows the AN^{•+} absorbance to rise monotonically from the zero (baseline) within the time (30 ps) of the laser pulse. Further temporal evolution of the 435-nm band was limited to a slight decrease in intensity (ca. 10%) during the time interval from 50 to 100 ps, after which it persisted

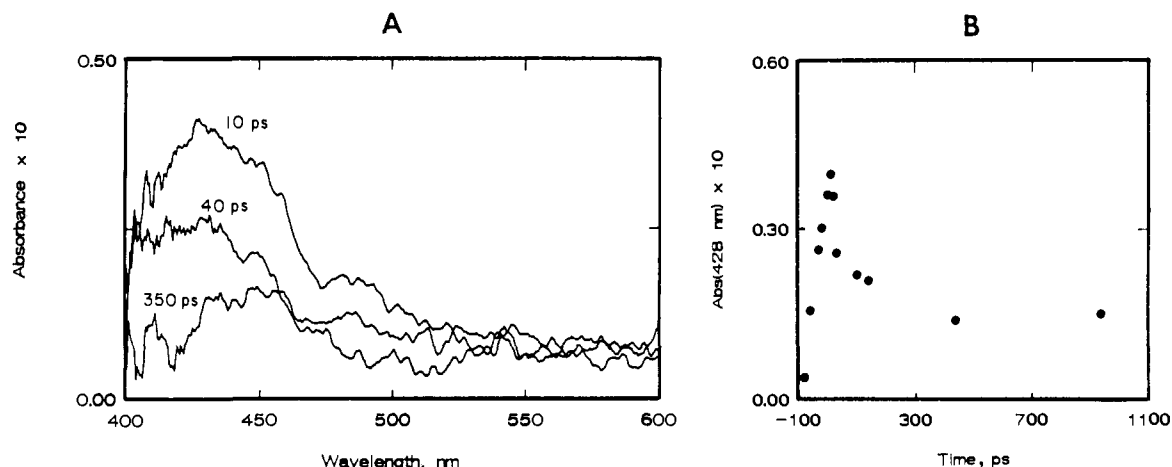


Figure 3. (A) Transient (difference) absorption spectra generated from the 355-nm irradiation of 0.4 M MeOPyNO₂⁺ in a mixture of toluene and acetonitrile (1:9 v/v) at 23 °C at the times indicated following the 30-ps (fwhm) laser pulse. (B) Temporal change of the absorbance at $\lambda_{\text{mon}} = 428$ nm showing a markedly reduced residual.

unchanged in shape and intensity throughout the monitoring period out to 5 ns.

Toluene. The charge-transfer excitation of the EDA complex of toluene (TOL) and *N*-nitro-4-methoxypyridinium in acetonitrile with the 30-ps laser pulse at $\lambda_{\text{exc}} = 355$ nm led to the series of time-resolved spectra shown in Figure 3A. The characteristic absorption spectrum with $\lambda_{\text{max}} = 430$ nm was identical to that of the toluene cation radical (TOL^{•+}) from previous reports.^{42,43} The temporal evolution of the toluene cation radical attendant upon the CT excitation of the [TOL, MeOPyNO₂⁺] complex followed at $\lambda_{\text{mon}} = 430$ nm showed a distinctly different pattern from that of the anisole analogue in Figure 2B. Thus, Figure 3B shows the spectral transient to reach maximum intensity within the risetime of the laser pulse, but, in contrast to the behavior of AN^{•+}, it was followed by a marked decrease over the time interval from 10 to 300 ps to a severely diminished (residual) absorbance that was only one-third of the maximum intensity. No further discernible change was noted in the weak residual absorbance between 300 ps and 5 ns.

Durene and Mesitylene. The time-resolved (picosecond) spectrum of durene cation-radical (DUR^{•+} with $\lambda_{\text{max}} = 465$ nm) generated via the 355-nm excitation of the EDA complex of durene (DUR) and *N*-nitro-4-methoxypyridinium in acetonitrile with a 30-ps laser pulse was the same as that previously produced by pulse radiolysis.⁴³ The temporal evolution of the durene cation radical followed the pattern established by AN^{•+}, the 465-nm absorbance of DUR^{•+} rising to a maximum and undergoing only a slight (<5%) subsequent decay out to 5 ns. On the other hand, the temporal behavior of the cation radicals of mesitylene (MES^{•+}, $\lambda_{\text{max}} = 465$ nm)⁴³ and *p*-xylene (XYL^{•+}, $\lambda_{\text{max}} = 440$ nm)⁴³ resembled that of TOL^{•+}, though with a more pronounced residual absorbance at 5 ns.

More generally, the residual absorbance of the aromatic cation radical produced upon CT excitation could be quantitatively expressed in a normalized form, i.e., $R = A_{\text{res}}/A_{\text{max}}$, where A_{max} was the maximum absorbance observed during the spectral

Table VI. Transient (Picosecond) Absorption Spectra and the Temporal Evolution of Aromatic Cation Radicals from the Charge-Transfer Excitation of EDA Complexes^a

aromatic donor ArH	M	MeOPyNO ₂ ^{•+} , ^b M	R ^c	$\lambda(\text{ArH}^{\bullet+})$, ^d nm	lit., ^e nm
anisole	0.36	0.026	0.9	435	435, ⁴¹ 445 ⁴¹
toluene	0.50	0.033	0.3	430	430, ⁴² 420 ²⁷
durene	0.20	0.030	0.9	465	465 ⁴³
mesitylene	0.24	0.033	0.5	455	460 ⁴³
<i>p</i> -xylene	0.54	0.028	0.6	440	440 ⁴³
hexamethylbenzene	0.06	0.055	1.0	495	495, ^{41,43} 500 ²⁷
benzene	2.0	0.050	0	428	427 ⁴²
biphenyl	0.09	0.04	<i>f</i>	680	690 ⁴⁴
4-bromoanisole	0.40	0.032	1.0	510	500 ¹³
4-methylanisole	0.36	0.026	1.0	445	450 ¹³
4-fluoroanisole	0.33	0.028	1.0	430	430, ¹³ 420 ⁴⁴

^a In acetonitrile solution by 355-nm CT excitation with 30-ps laser pulse at 23 °C. ^b As tetrafluoroborate salt. ^c Residual fraction (see text). ^d Absorption maximum. ^e Superscript represents the literature citation as reference numbers. ^f Not determined.

evolution. The values of *R* evaluated in this manner ranged from *R* = 1.0 for cation radicals derived from the electron-rich donors hexamethylbenzene and bromoanisole to represent no absorbance diminution on the picosecond time scale to *R* = 0.3 from toluene to indicate substantial but incomplete decay of TOL^{•+} (see Figure 3B). The transient absorption spectra of the aromatic cation radicals from the charge-transfer excitation of various EDA complexes with MeOPyNO₂⁺ are collected in Table VI,^{40–44} together with values of the residual fraction.

IV. Quantum Efficiency for the CT Generation of Aromatic Cation Radicals from the EDA Complex. In order to quantify the production of the anisole cation radicals (at the temporal plateau shown in Figure 2B), the charge-transfer excitations were carried out with a second spectrometric unit that consisted of a Q-switched Nd³⁺:YAG laser with 10-ns (fwhm) resolution for spectral observations extending down into the microsecond region. Thus the transient (ns) spectra in Figure 4A show the principal absorption band of the anisole cation radical with $\lambda_{\text{max}} = 435$ nm corresponding to that in the picosecond spectra in Figure 2A. Owing to the persistence of AN^{•+} on the ns time scale, the quantum yield Φ for its formation could be readily measured by the method of relative actinometry⁴⁵ based on the benzophenone triplet ($\lambda_{\text{max}} = 530$ nm)⁴⁶ as the transient actinometer. The value of $\Phi = 0.82 \pm 0.05$ was determined in the time interval: $10 < t < 100$ ns after the CT excitation of the anisole complex with *N*-nitro-4-

(44) Lemmetyinen, H.; Konijnenberg, J.; Cornelisse, J.; Varma, C. A. G. *O. J. Photochem.* **1985**, *30*, 315.

(45) Bonneau, R.; Carmichael, I.; Hug, G. L. *Pure Appl. Chem.* **1991**, *63*, 289.

(46) Hurley, J. K.; Sinai, N.; Linschitz, H. *Photochem. Photobiol.* **1983**, *38*, 9.

(37) Barnes, C. E.; Feldman, K. S.; Johnson, M. W.; Lee, H. W. H.; Myhre, P. C. *J. Org. Chem.* **1979**, *44*, 3925.

(38) Friedel, R. A.; Orchin, M. *Ultraviolet Spectra of Aromatic Compounds*; Wiley: New York, 1951.

(39) Note the segmental shifts in the spectral envelope at $t < 10$ ps was an instrumental artifact caused by temporal dispersion (chirp) associated with the group velocities of the various probing wavelengths. See: Masuhara, H.; Miyasaka, H.; Karen, T.; Uemiyama, T.; Mataga, N.; Koishi, M.; Takeshima, A.; Tsuchiya, Y. *Opt. Commun.* **1984**, *44*, 426.

(40) Takamaku, S.; Komitsu, S.; Toki, S. *Radiat. Phys. Chem.* **1989**, *34*, 553.

(41) Shida, T. *Electronic Absorption Spectra of Radical Ions*; Elsevier: New York, 1988; p 254.

(42) Dymerski, P. P.; Fu, E.; Dunbar, R. *J. Am. Chem. Soc.* **1974**, *96*, 4109.

(43) Sehested, K.; Holcman, J.; Hart, E. J. *J. Phys. Chem.* **1977**, *81*, 1363.

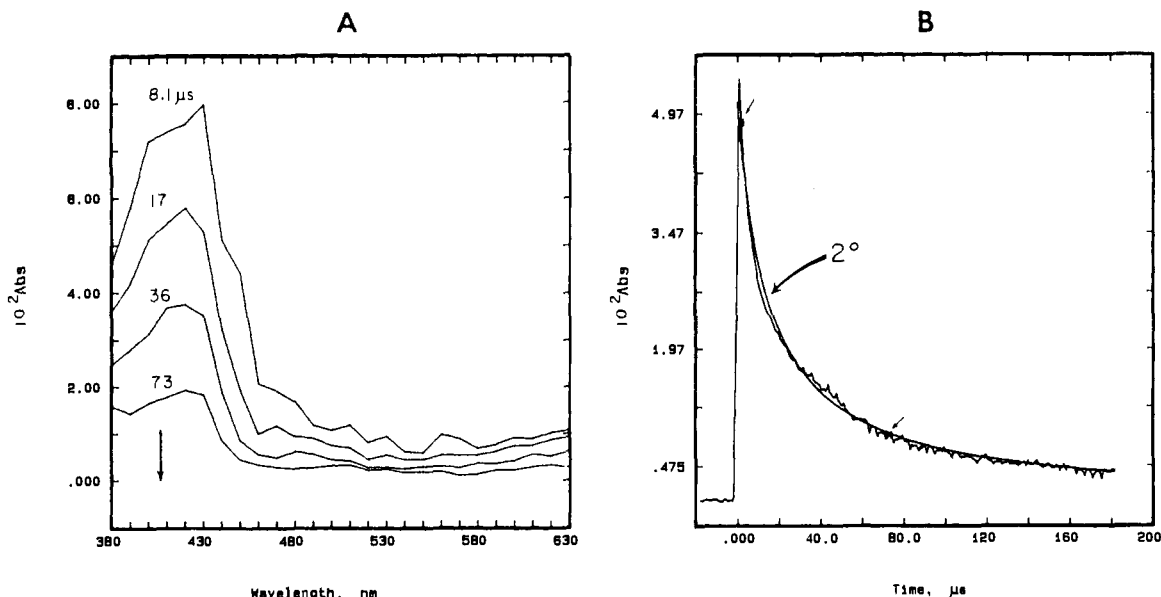


Figure 4. (A) Time-resolved (nanosecond) absorption spectra of the anisole cation radical following the 355-nm irradiation of the anisole/MeOPyNO₂⁺ complex in acetonitrile with a 10-ns (fwhm) laser pulse (recorded at the indicated times). (B) Spectral decay of AN⁺⁺ monitored at 440 nm, with the smooth curve representing the computer-generated fit of the data to second-order kinetics.

Table VII. Quantum Yields for the Generation of Transient Aromatic Cation Radicals on the Nanosecond Time Scale^a

aromatic donor	λ_{mon} , nm	ϵ , M ⁻¹ cm ⁻¹	Φ
anthracene	715	12500 ^b	0.72
naphthalene	580	3600	0.82 ^c
anisole	435	4800	0.80
hexamethylbenzene	495	1800 ^d	0.56
durene	465	1800 ^d	0.56
<i>p</i> -xylene	440	2050 ^d	0.25
toluene	435	2000 ^d	0.14

^a Generated by CT photolysis (355 nm) of the EDA complex formed by the aromatic donor (0.05–0.2 M) and MeOPyNO₂⁺BF₄⁺ (0.025–0.04 M) in acetonitrile at 23 °C using benzophenone triplet as the transient actinometer. ^{b-d} From ref 66 (b), 17 (c), and 43 (d).

methoxy-pyridinium in acetonitrile at 23 °C. For comparison, Table VII includes the quantum yields for the formation of toluene, durene, and other aromatic cation radicals pertinent to charge-transfer nitration via the 355-nm excitation of the corresponding EDA complexes with the 10-ns laser pulse. It is important to note that $\Phi = 0.8$ for anisole is consistent with the picosecond results in Table VI that show negligible decay of the AN⁺⁺. Furthermore, the decreasing values of Φ for the various methylbenzenes, viz., HMB⁺⁺ \approx DUR⁺⁺ > XYL⁺⁺ > TOL⁺⁺ in Table VII occur in the same decreasing order of the residuals R listed in Table VI.

V. Temporal Evolution of Anisole and Related Cation Radicals.

The subsequent disappearance of anisole cation radical was observed as the uniform decay of the absorption band in Figure 4A to the spectral baseline within 200 μ s—to yield finally a residual spectrum with only a minor absorptions. The adherence of the absorbance change ($A_0 - A$) at $\lambda_{\text{max}} = 435$ nm to second-order kinetics was clearly indicated by the precise fit of the computer-generated (smooth) line, as typically shown in Figure 4B. [Note the time interval for the least-squares treatment is bracketed by the pair of asterisks.] The second-order decay was also confirmed by (a) the constancy of the rate constant $k_{11} = 1.1 \pm 0.3 \times 10^6$ A⁻¹ s⁻¹ evaluated in this manner by variation in the initial absorbance A_0 (proportional to the laser power) as well as (b) the inverse variation of the apparent half-life (τ) with A_0 in Table VIII.⁴⁷ The experimental second-order rate constant in Table VIII measured directly in absorbance units from the CT excitation of the anisole complex with *N*-nitro-4-methoxy-pyridinium was

Table VIII. Second-Order Kinetics for the Decay of AN⁺⁺^a

A_0^b ($\times 100$)	half-life, ^c μ s	k_{11}^d 10^6 A ⁻¹ s ⁻¹	A_0^b ($\times 100$)	half-life, ^c μ s	k_{11}^d 10^6 A ⁻¹ s ⁻¹
3.8	32	0.83	6.9	10	1.2
4.5	22	1.2	7.2	12	1.0
4.9	14	1.3	8.1	11	1.3
5.3	13	1.1	8.3	10	1.1

^a Generated by 355-nm CT photolysis of the EDA complex formed from anisole (0.1–0.2 M) and MeOPyNO₂⁺BF₄⁺ (0.03–0.04 M) in MeCN at 23 °C. ^b Initial absorbance at 440 nm. ^c Time for an absorbance to decrease to $1/2 A_0$. ^d Second-order rate constant in absorbance units.

equivalent to the standard second-order rate constant $k_{11} = 4.8 \pm 0.8 \times 10^9$ M⁻¹ s⁻¹ with the extinction coefficient $\epsilon_{435} = 4400$ M⁻¹ cm⁻¹ was used for the 435-nm absorbance of AN⁺⁺. It is noteworthy that the analogous spectral decay from the 532-nm CT excitation of the corresponding tetranitromethane complex (vide supra) obeyed the same second-order kinetics—with the value of $k_{11} = 3.0 \pm 0.8 \times 10^9$ M⁻¹ s⁻¹ being experimentally indistinguishable from that evaluated from the nitropyridinium complex (see Table VIII). In both cases, the stoichiometry from charge-transfer nitration in eqs 3 and 4 allowed the spectral decay of the anisole cation radical to be assigned to its common reaction with NO₂ (vide infra). The accompanying spectral decay of the latter was not observed owing to the nondescript (diffuse) NO₂ absorption.^{48,49}

The deuterium kinetic isotope effect on the disappearance of anisole cation radical was determined from the CT excitation of anisole-*d*₅ and *N*-nitro-4-methoxy-pyridinium. Under the reaction conditions described in Table IX, the second-order rate constants k_{obs} for AN⁺⁺ and AN-*d*₅⁺⁺ were found to be the same within the experimental uncertainty. Table IX also includes the observed second-order rate constants for the decay of the aromatic cation radicals derived from the 355-nm excitation of the EDA complexes of *N*-nitro-4-methoxy-pyridinium with the various 4-substituted haloanisoles examined in the previous study.¹³

VI. Spectral Decay of Aromatic Cation Radicals in the Presence of Additives. In order to obtain further information about the chemical process(es) responsible for the second-order decay in Figure 4, the disappearance of AN⁺⁺ was monitored in the presence of two particular additives.

(a) **Nitrogen dioxide** was vacuum transferred into a dual compartment photochemical/electrochemical cell of local

(47) Moore, J. W.; Pearson, R. G. *Kinetics and Mechanism*, 3rd ed.; Wiley: New York, 1981; p 60.

(48) Hall, T. C., Jr.; Blacet, F. E. *J. Chem. Phys.* **1952**, *20*, 1745.

(49) Gillispie, G. D.; Kahn, A. U. *J. Chem. Phys.* **1976**, *65*, 1624.

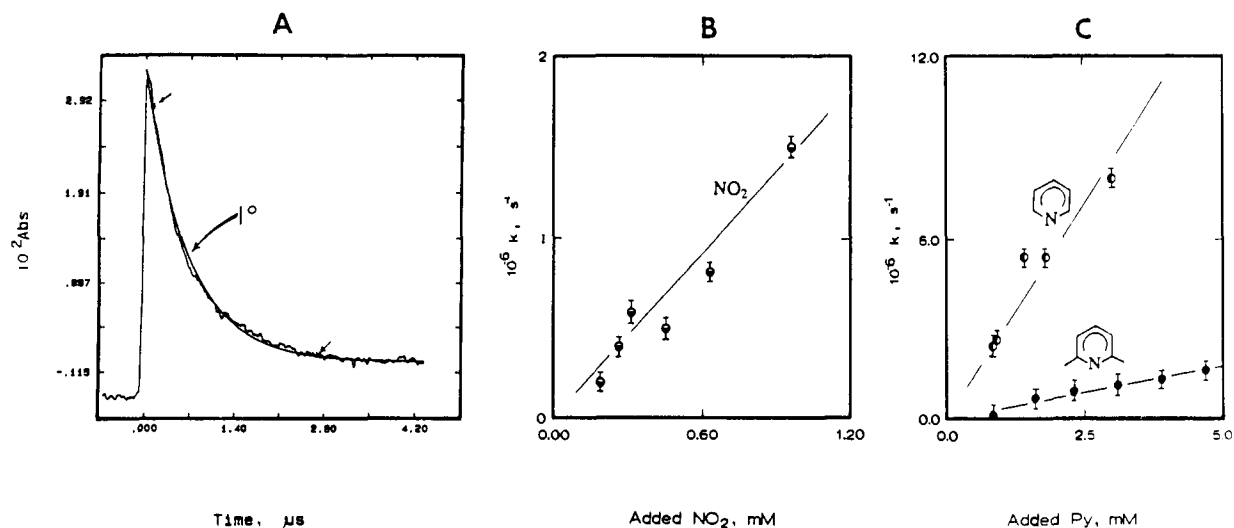


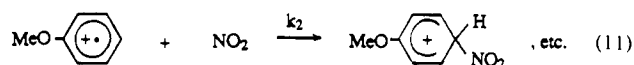
Figure 5. (A) Typical decay of anisole cation radical in the presence of added NO_2 , showing the fit to first-order kinetics (smooth curve). [$\text{AN}^{\bullet+}$ generated from the 355-nm irradiation of 0.2 M anisole and 0.03 MeOPyNO_2^+ in acetonitrile.] (B) Plot of the pseudo-first-order rate constant against the concentration of added NO_2 . (C) Similar to (B), but with added pyridine or 2,6-lutidine.

Table IX. Second-Order Rate Constants for the Spectral Decay of Aromatic Cation Radicals Following the CT Excitation of $[\text{ArH}^{\bullet+}, \text{MeOPyNO}_2^+]$ Complexes^a

aromatic donor	M	$\lambda_{\text{mon}},^b$ nm	$k_{11},^{c,d}$ $10^9 \text{ M}^{-1} \text{ s}^{-1}$
anisole	0.2–0.4	440	4.8 (3)
anisole- <i>d</i> ₅	0.2–0.5	440	4.7
<i>p</i> -methylanisole	0.05–0.2	450	1.6 (1.3)
<i>p</i> -bromoanisole	0.08–0.3	510	2.0 (2)
<i>p</i> -chloroanisole	0.1–0.3	470	1.4 (1.4)
<i>p</i> -fluoroanisole	0.1–0.3	430	4.0

^a Decay kinetics of cation radicals generated by CT photolysis of the EDA complex of the aromatic donor with MeOPyNO_2^+ (0.02–0.05 M) as the tetrafluoroborate salt or TNM (0.2–0.5 M) in acetonitrile at 23 °C. ^b Monitoring wavelength. ^c Second-order rate constant obtained from the absorbance decays following the 355-nm excitation of the EDA complex with MeOPyNO_2^+ . ^d In parenthesis, the second-order rate constant for decay of the same cation radical generated by 532-nm CT photolysis of the EDA complex with TNM.

design⁵⁰ that contained the predetermined amounts of anisole and MeOPyNO_2^+ in acetonitrile solution. The concentration of dissolved nitrogen dioxide was measured in situ by linear sweep voltammetry using a platinum microelectrode (see the supplementary material for the details of the analysis). Under these conditions, the spectral decay of anisole cation radical obeyed pseudo-first-order kinetics to beyond four half-lives (see Figure 5A). The rate constant followed a first-order dependence on the concentration of nitrogen dioxide $[\text{NO}_2]$, as illustrated in Figure 5B. The overall second-order rate constant ($k_2 = 1.5 \times 10^9 \text{ M}^{-1} \text{ s}^{-1}$) evaluated from the slope thus represented its homolytic annihilation by the aromatic cation radical, i.e.



The reactivity of other aromatic cation radicals with NO_2 was also examined by the same pseudo-first-order method described above. Interestingly, the second-order rate constants were encompassed within only a limited span of $(0.5 \times 10^9) < k_2 < (1.5 \times 10^9) \text{ M}^{-1} \text{ s}^{-1}$, despite the relatively wide range of the cation-radical stabilities included in Table X (column 2).⁵¹

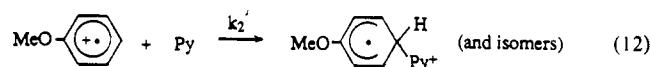
(b) **Pyridine** was typically added in incremental amounts to a photochemical cell that contained anisole and tetranitromethane dissolved in acetonitrile. Attendant upon the 532-nm excitation

Table X. Second-Order Reactions of Aromatic Cation Radicals with Nitrogen Dioxide, Pyridine, or 2,6-Lutidine^a

aromatic donor	IP, eV	second-order rate constant, $10^9 \text{ M}^{-1} \text{ s}^{-1}$		
		$k_2(\text{NO}_2)^b$	$k_2'(\text{Py})^c$	$k_2'(\text{Lut})^d$
anisole	8.39	1.5	2.5	0.3
mesitylene	8.42		0.3	0.05
<i>p</i> -bromoanisole	8.3	1.0	0.1	0.06
<i>p</i> -chloroanisole	8.4	1.0	0.06	0.05
<i>p</i> -xylene	8.44	0.5		
toluene	8.82	1.0		
naphthalene ^e	8.12	4.0	0.38	0.08
biphenyl	8.45	1.5		

^a In acetonitrile at 23 °C. ^{a-d} Aromatic cation radical ($\text{ArH}^{\bullet+}$) generated by CT excitation of the aromatic EDA complex from MeOPyNO_2^+ (b) with added pyridine (c) or 2,6-lutidine (d) at 532 nm. ^e From ref 17.

of the EDA complex, the spectral decay of anisole cation radical followed clean first-order kinetics to beyond four half-lives in a manner similar to that illustrated in Figure 5A. Figure 5C shows the linear dependence of the pseudo-first-order rate constant on the concentration of added pyridine, and the second-order rate constant $k_2' = 2.5 \times 10^9 \text{ M}^{-1} \text{ s}^{-1}$ thus represented the nucleophilic addition of pyridine to the aromatic cation radical, i.e.⁵²



This conclusion is supported in Figure 5C by the slower rate of the sterically hindered 2,6-lutidine which is a weaker nucleophile but stronger base than pyridine.^{53,54}

Discussion

The photochemical nitrations of common aromatic donors including anisole, toluene, etc., as included in Tables II–V, are efficiently carried out with *N*-nitropyridinium by the deliberate irradiation of the charge-transfer absorption bands—especially at (low) temperatures where the more common electrophilic aromatic nitration¹⁶ is too slow to compete. From a mechanistic perspective, such a photoinduced process allows the use of time-resolved spectroscopic methods to directly establish the reactive

(50) Bockman, T. M.; Karpinski, Z.; Sankaraman, S.; Kochi, J. K. *J. Am. Chem. Soc.* **1992**, *114*, 1970.

(51) Since the formation energy of neutral aromatic donors is invariant relative to the cation radical, the values of E_{red} follow the trend in $\text{ArH}^{\bullet+}$ stabilities.^{12a}

(52) Yoshida, K. *Electrooxidation in Organic Chemistry*; Wiley: New York, 1984; pp 65, 82, 85–86.

(53) Fischer, A.; Galloway, W. J.; Vaughan, J. *J. Chem. Soc.* **1964**, 3591.

(54) Cauquis, G.; Deronzier, A.; Serve, D.; Vieil, E. *J. Electroanal. Chem.* **1975**, *60*, 205.

intermediates responsible for charge-transfer (CT) nitration in the following way.

I. Charge-Transfer Activation of Aromatic EDA Complexes with *N*-Nitropyridinium. Spontaneous Formation of the Aromatic Cation Radical in the Reactive Triad. The charge-transfer absorptions in Table I demonstrate the presence of aromatic EDA complexes with *N*-nitropyridinium (see eq 1) as the first-formed intermediate. Time-resolved (picosecond) spectroscopy immediately following the application of the laser-pulse then identifies the direct photoexcitation ($h\nu_{CT}$) of the aromatic EDA complex with the spontaneous formation of the reactive triad, i.e.^{8,13}

Scheme I



Thus Figures 2A and 3A show the typical absorption spectra of the aromatic cation radicals ($\text{ArH}^{+\bullet}$) obtained upon the application of the laser pulse ($h\nu_{CT}$). The appearance of the absorption spectra of $\text{ArH}^{+\bullet}$ (eq 14) that is coincident with the characteristic risetime of the laser pulse accords with the expectations of Mulliken theory of charge-transfer.^{11,12} [Note the parallel spectral growth of the accompanying nitropyridinyl radical (not observed directly⁵⁵) is demanded by chemical stoichiometry.]

The facile reversion of the aromatic cation radical by back electron transfer (k_{bet} in eq 14) is a common pathway for the deactivation of CT-generated ion radical pairs;⁵⁶ and it is spectrally manifested in the two typical (biphasic) profiles shown in Figures 2B and 3B for the cation radicals from anisole (AN) and toluene (TOL), respectively. Thus $\text{AN}^{+\bullet}$ suffers only a minor (overall) diminution on the picosecond timespan and its absorbance attains a high residual R (Table VI), which is markedly diminished in the case of $\text{TOL}^{+\bullet}$; and the previous study⁵⁵ establishes these distinctive rate profiles to result from the rapid fragmentation (k_f) of the accompanying *N*-nitropyridinyl radical in eq 15 that diverts the aromatic cation radical from back electron transfer.⁵⁷ Such a competition is quantitatively evaluated from the (nanosecond) quantum yields in Table VII as⁵⁰

$$\Phi \approx k_f / (k_{\text{bet}} + k_f) \quad (16)$$

Based on this relationship and the estimated value of $k_f \sim 3 \times 10^{11} \text{ s}^{-1}$,⁵⁵ the back electron-transfer rates for $\text{AN}^{+\bullet}$ and $\text{TOL}^{+\bullet}$ in eq 14 are calculated to be $k_{\text{bet}} = 8 \times 10^{10}$ and $2 \times 10^{12} \text{ s}^{-1}$, respectively.

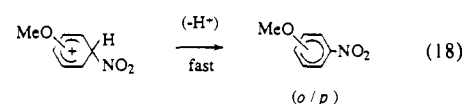
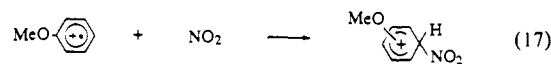
II. Temporal Evolution of Aromatic Cation Radicals to the Wheland Intermediate and the Nucleophilic Adduct. The observation of second-order kinetics (k_{11}) for the spectral decay of the anisole cation radical in Figure 4 (see Table VIII) points to the disappearance of $\text{AN}^{+\bullet}$ after its separation from the initially formed triad in eq 15. Owing to the high yields of nitroanisoles obtained (Table II), such a process can be formulated as the bimolecular (homolytic) reaction in eq 17 that produces the critical Wheland intermediate in aromatic nitration according to Perrin⁵⁸ and Ridd,⁵⁹ i.e.

(55) Bockman, T. M.; Lee, K. Y.; Kochi, J. K. *J. Chem. Soc., Perkin Trans. 2* **1992**, 1581.

(56) Mattay, J.; Vondenhof, M. *Top. Curr. Chem.* **1991**, *159*, 219.

(57) (a) Fox, M. A. *Adv. Photochem.* **1986**, *13*, 237. (b) Weller, A. *Pure Appl. Chem.* **1982**, *54*, 1885. (c) Suppan, P. *Top. Curr. Chem.* **1992**, *163*, 95.

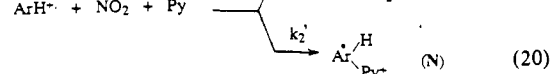
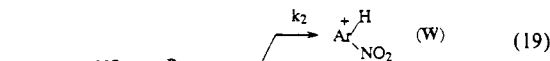
Scheme II



Most importantly, the direct reaction of anisole cation radical with NO_2 (eq 17) is established by the pseudo-first-order kinetics observed for the disappearance of $\text{AN}^{+\bullet}$ in the presence of added NO_2 (see Figure 5A). The magnitude of the second-order rate constant of $k_2 = 1.5 \times 10^9 \text{ M}^{-1} \text{ s}^{-1}$ evaluated in this way is thus consistent with the spectral decay of the freely diffusing aromatic cation radical ($\text{AN}^{+\bullet}$) in Figure 4.⁶⁰

According to Scheme II, the isomeric (ortho/para) product ratios are established during the collapse of the radical pair in eq 17 (most likely at the positions of $\text{AN}^{+\bullet}$ with the highest electron density⁶¹). Furthermore, the absence of a measurable kinetic isotope effect in the decay of the deuterated analogue ($\text{C}_6\text{D}_5\text{-OCH}_3^+$) in Table IX is predicted from Scheme II since the proton loss occurs in a subsequent, rapid step (eq 18).⁶² The absence of a deuterium kinetic isotope effect also indicates that the presence of pyridine in the triad (eq 15) does not lead to the nitroanisoles by an alternative pathway involving the prior deprotonation of the anisole cation radical followed by a free-radical coupling with NO_2 . Pyridine, however, cannot be an innocent bystander in the charge-transfer nitration of anisole, since the second-order rate constant that is evaluated for the disappearance of $\text{AN}^{+\bullet}$ in the presence of added Py is comparable to that obtained in the presence of added NO_2 (compare k_2' and k_2 in Table X). Moreover, the significantly slower rate obtained with the sterically hindered (but stronger base) 2,6-lutidine in Figure 5C is consistent with nucleophilic addition to $\text{AN}^{+\bullet}$, as presented in eq 12.^{44,63,64} In other words, the triad of reactive fragments produced in eq 15 in the CT excitation of the EDA complex with *N*-nitropyridinium is susceptible to mutual (pairwise) annihilations leading to the Wheland intermediate (W) and the nucleophilic adduct (N), i.e.

Scheme III



so that the observed second-order rate constants k_{11} for the spectral decay of $\text{ArH}^{+\bullet}$ in Table IX actually represents a composite of k_2' and k_2 .⁶⁵ A similar competition between the homolytic and nucleophilic reactivity of aromatic cation radicals is observed in the reactive triad from charge-transfer nitrations with tetranitromethane, i.e.¹³

(58) Perrin, C. L. *J. Am. Chem. Soc.* **1977**, *99*, 5516.

(59) Ridd, J. H. *Chem. Soc. Rev.* **1991**, *20*, 149.

(60) See: Garst, J. F. *J. Chem. Soc., Faraday Trans. 1* **1989**, *85*, 1245.

(61) Pedersen, E. B.; Petersen, T. E.; Torssell, K.; Lawesson, S. O. *Tetrahedron* **1973**, *29*, 579. See, also: Epiotis, N. D. *J. Am. Chem. Soc.* **1973**, *95*, 3188.

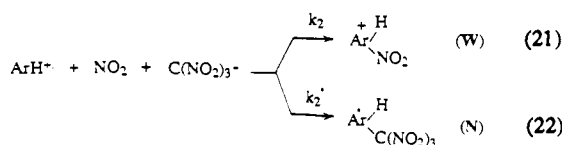
(62) Melander, L. *Arkiv. Kemi* **1950**, *2*, 211; **1957**, *11*, 77. See, also: Melander, L. *Isotope Effects on Reaction Rates*; Ronald Press: New York, 1960.

(63) (a) Schlesener, C. J.; Kochi, J. K. *J. Org. Chem.* **1984**, *49*, 3142. (b) For the direct (spectroscopic) observation of the nucleophilic adduct N during CT activation, see: supplementary material. (c) By contrast, the fast deprotonation of the Wheland intermediate precludes its spectral observation on the time scale in Table IX.

(64) (a) Reitstoen, B.; Parker, V. D. *J. Am. Chem. Soc.* **1991**, *113*, 6954. (b) Hammerich, O.; Parker, V. D. *Adv. Phys. Org. Chem.* **1984**, *20*, 55. (c) Parker, V. D. *Acc. Chem. Res.* **1984**, *17*, 243.

(65) (a) The observed second-order rate constant k_{11} is approximated by ($k_2 + k_2'$) for the first few half-lives, as described in the supplementary materials. (b) For the dual (homolytic and nucleophilic) reactivities of aromatic cation radicals, see Sankararaman et al. in ref 13.

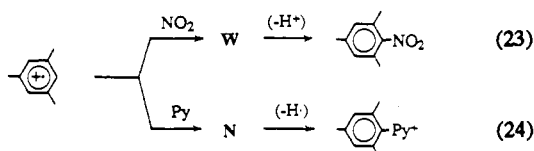
Scheme IV



Since the uncharged nucleophilic adduct in Scheme IV arises from the ion-pair annihilation of an anionic nucleophile (trinitromethide), the rate constant (k_2' in eq 22) is strongly dependent on the solvent polarity.⁶⁶

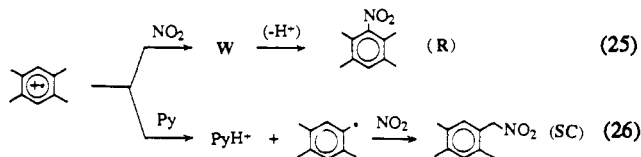
The simultaneous annihilation of the aromatic cation radical by its triad partners NO_2 and Py , as presented in Scheme III, is most apparent in the nature of the aromatic product (i.e., stoichiometry) from mesitylene, among all the other aromatic donors included in Tables II–V. Thus, the direct incorporation of NO_2 and Py into the aromatic nucleus is shown by the concomitant ring nitration and pyridination of mesitylene (in eq 6 and Table IV, entry 11), which clearly derive from the Wheland intermediate (W) and nucleophilic adduct (N), respectively, i.e.⁶⁷

Scheme V



A similar (but somewhat less obvious) dichotomy results in the simultaneous ring and side-chain substitution of durene in eq 5. Thus in this charge-transfer nitration, the addition of NO_2 to the cation radical $\text{DUR}^{\cdot+}$ (eq 25) occurs in competition with its deprotonation (eq 26), in which the pyridine has been shown to act as a base,⁶⁸ i.e.

Scheme VI



[Note that deprotonation of $\text{DUR}^{\cdot+}$ also leads to aromatic dimers (D) via the subsequent (oxidative) substitution of the benzylic radical formed in eq 26.²⁸]

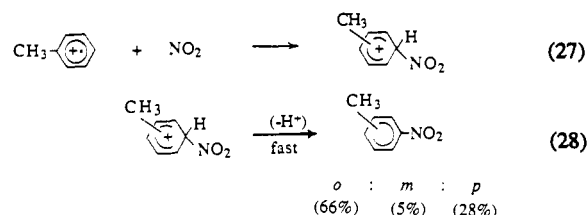
III. Mechanism of Charge-Transfer Nitration. The ambiphilic reactivity of aromatic cation radicals, as described in Schemes III and IV, is particularly subtle in the charge-transfer nitration of toluene and anisole, which afford uniformly high (>95%) yields of only isomeric nitrotoluenes and nitroanisoles, respectively, without the admixture of other types of aromatic byproducts. Accordingly, let us consider how the variations in the isomeric (ortho/meta/para) product distributions with different nitrating agents (NO_2Y) provide unique mechanistic insights into charge-transfer nitration of each of these aromatic donors.

Toluene. The distinctive pattern of *o*-, *m*-, and *p*-nitrotoluenes produced in Table III is strongly dependent on the *N*-nitropyridinium reagent and the presence of additives as follows. (i) $\text{Me}_2\text{PyNO}_2^+$ (derived from the sterically hindered 2,6-lutidine base) yields primarily *o*- and *p*-nitrotoluene on a more or less statistical basis (entry 1). (ii) MeOPyNO_2^+ (derived from the relatively strong 4-methoxypyridine base) leads to a nitrotoluene mixture that is unusually rich in the meta isomer (60% in entry 5). (iii) MeOPyNO_2^+ in the presence of added NO_2 (entry 10) leads to the complete restoration of the statistical ortho/para

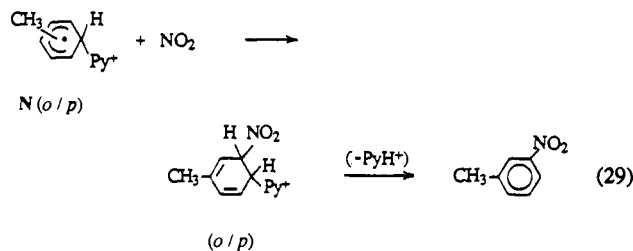
pattern of (i)—with minimal amounts of the meta isomer that are otherwise produced in (ii). (iv) MeOPyNO_2^+ in the presence of added trifluoroacetic acid (TFA entry 8) has a tendency to enhance the ortho and para isomers at the expense of high meta, but less effectively than in (iii). (v) $\text{C}(\text{NO}_2)_4$ (entry 12) also leads to a nitrotoluene mixture that is unusually rich in the meta isomer [though less than that from MeOPyNO_2^+ in facet (ii)].

The facet (iii) above, taken in the context of the triad annihilation in Scheme III, indicates that the more or less statistical ortho/para pattern is diagnostic of the homolytic pathway (eq 19) since it will dominate the competition for $\text{TOL}^{\cdot+}$ at the high concentrations of added NO_2 , i.e.

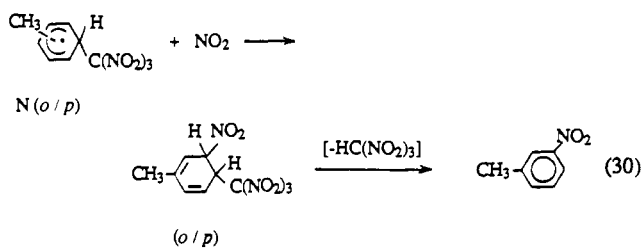
Scheme VII



Indeed this conclusion is supported by facet (i), in which essentially the same isomeric product distribution (i.e., ortho/meta/para = 70, 2, 28%) is achieved when the pyridine competition is thwarted for the sterically hindered 2,6-lutidine, an ineffective nucleophile.^{63,64} According to the formulation in Scheme VII, the isomeric product distribution is established from the sterically hindered $\text{Me}_2\text{PyNO}_2^+$ during the homolytic annihilation of $\text{TOL}^{\cdot+}$ by NO_2 , most favorably at the ortho and para positions to accord with the experimental (ESR) and theoretical charge densities in the toluene cation radical.⁶⁹ We are thus left with facets (ii) and (iv) to clearly point out the direct role of the pyridine in the (extra) meta-substitution of toluene during CT nitration with MeOPyNO_2^+ . Since such an extrinsic pathway must proceed via the nucleophilic adduct (eq 20), a direct route to *m*-nitrotoluene involves the trapping of N by NO_2 , followed by elimination, e.g.⁷⁰



and a similar formulation can account for the high meta nitration with tetranitromethane in facet (v), i.e.



The formation of cyclohexadiene adducts in eqs 29 and 30 by such a sequence of addition steps⁷¹ and the rearomatization to afford substitution products⁷² is known for various aromatic systems.⁷³

(66) Yabe, T.; Kochi, J. K. *J. Am. Chem. Soc.* **1992**, *114*, 4491.

(67) (a) For the homolytic annihilation and rapid deprotonation in eq 23, see Sankararaman et al. in ref 13. (b) Hydrogen atom loss in eq 24 probably occurs via a two-step (oxidation/deprotonation) sequence.^{63,64}

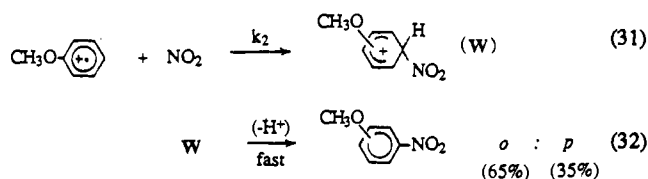
(68) See: Masnovi, J. M., et al. in ref 27.

(69) (a) Komatsu, T.; Lund, A.; Kinell, P.-O. *J. Phys. Chem.* **1972**, *76*, 1721. (b) Rao, D. N. R.; Symons, M. C. R. *J. Chem. Soc., Perkin Trans.* **2** **1985**, 991. (c) See, also: Chandra, H.; Symons, M. C. R.; Hasegawa, A. *J. Chem. Soc., Faraday Trans. 1* **1987**, *83*, 759.

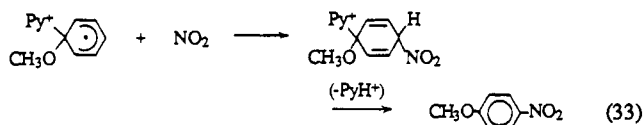
Anisole. The simultaneous (homolytic and nucleophilic) annihilations of $AN^{+\bullet}$ as described by the time-resolved spectroscopic results in eqs 11 and 12 lead to the distinctive mixtures of *o*- and *p*-nitroanisoles, in Table II, in which the isomeric composition is strongly dependent on the nitrating reagent in the following way. (i) $Me_2PyNO_2^+$ (entry 1) yields a (nearly) statistical mixture of *o*- and *p*-nitroanisole. (ii) $MeOPyNO_2^+$ (entry 7) leads to a nitroanisole mixture that is unusually rich in the para isomer—such that the isomeric product distribution is reversed relative to that in (i). (iii) $C(NO_2)_4$ (entry 10) also affords an ortho/para mixture like that from $MeOPyNO_2^+$ in (ii), in which the para isomer predominates.

The triad annihilations in Schemes III and IV again provide the mechanistic basis for analyzing these apparently disparate results. Thus the difference between $Me_2PyNO_2^+$ and $MeOPyNO_2^+$ in facets (i) and (ii), respectively, mirrors that observed for toluene (vide supra). We accordingly attribute the statistical ortho/para pattern obtained from $Me_2PyNO_2^+$ in facet (i) to a similar dominance of the homolytic annihilation of $AN^{+\bullet}$ to produce the critical Wheland intermediate in aromatic nitration, i.e.

Scheme VIII



Indeed, the ineffectiveness of the sterically hindered 2,6-lutidine to provide the nucleophilic competition for the triad in Scheme III is shown by the relative magnitudes of the second-order rate constants k_2 and k_2' in Table X.⁷⁴ Based on experiment (ESR) and theoretical studies,⁷⁵ the homolytic annihilation of $AN^{+\bullet}$ by NO_2 occurs at the positions of highest charge density and produces the statistical mixture of *o*- and *p*-nitroanisoles in eq 32. If so, the additional *p*-nitroanisole produced in facet (ii) is associated with the increased competition from nucleophilic addition arising from the presence of the electron-rich 4-methoxypyridine ($MeOPy$) in the triad. Under these circumstances, the nucleophilic adduct N, which is responsible for the (extra) *p*-nitroanisole, may arise via an ipso addition, followed by the usual addition/elimination sequence, i.e.



As such, the isomeric adduct formed by the nucleophilic addition to $AN^{+\bullet}$ at the ortho/para positions may be responsible for the minor amounts of *m*-nitroanisole (compare eq 29) since it is

(70) (a) Nucleophilic addition to $TOL^{+\bullet}$, like homolytic addition, is favored at the *o/p* positions.¹⁰⁰ (b) The increase in *m*-nitrotoluene, mainly the expense of the ortho isomer (para relatively unchanged) in Table III (entries 5 and 9, etc.) may be attributed an addition/elimination pathway at the ipso position similar to that for anisole ion (see eq 33).

(71) Masnovi, J. M.; Kochi, J. K. *J. Am. Chem. Soc.* **1985**, *107*, 7880. See, also: Ebersson, L.; Hartshorn, M. P. *J. Chem. Soc., Chem. Commun.* **1992**, 1563.

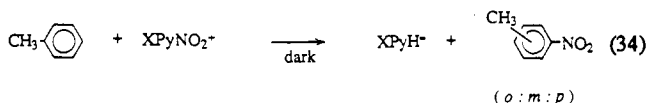
(72) (a) Fischer, A.; Wilkinson, A. L. *Can. J. Chem.* **1972**, *50*, 3988. (b) Fischer, A.; Ramsay, J. N. *Can. J. Chem.* **1974**, *52*, 3960. (c) Fischer, A.; Goel, A. J. *Chem. Soc., Chem. Commun.* **1988**, 526. (d) Fischer, A.; Röderer, R. *J. Chem. Soc., Chem. Commun.* **1975**, 798. (e) Bockman, T. M.; Kim, E. K.; Kochi, J. K. *Bull. Soc. Chim. Fr.*, in press. See, also: Kim et al. in ref 17.

(73) Meta substitution of toluene (and para substitution of anisole) via the elimination of cyclohexadiene adducts have been previously postulated in aromatic nitration by Rudakov, E. S.; Lobachev, V. L.; Savsunenko, O. B. *Kinet. Katal. (Engl. Trans.)* **1991**, *31*, 938. Compare, also *m*-acetoxylation: Henry, P. M. *J. Org. Chem.* **1971**, *36*, 1886. Ebersson, L.; Gomez-Gonzalez, L. *Acta Chem. Scand.* **1973**, *27*, 1249.

observed mainly with the best nucleophiles (see Table II, entries 6 and 10). The same pattern of *o*-, *m*-, and *p*-nitroanisoles obtained with tetranitromethane in facet (iii) follows from an analogous competition between homolytic and ion-pair (nucleophilic) annihilations in Scheme IV.¹³ The preferential addition of both $MeOPy$ and $C(NO_2)_3^-$ as nucleophiles to the ipso center of $AN^{+\bullet}$ is predicted from the high charge density at this position^{75a} (less significant charges lie at the ortho/para positions of $AN^{+\bullet}$).^{75b,76} Thus, the difference between the aromatic cation radicals $AN^{+\bullet}$ and $TOL^{+\bullet}$ is sufficient to alter the principal nitration product arising from their nucleophilic annihilation from para (eq 33) to the meta isomer (eq 29). In the absence of such an extraneous pathway, the direct CT nitration of anisole and toluene via the homolytic annihilation of $AN^{+\bullet}$ and $TOL^{+\bullet}$ in Schemes VII and VIII, respectively, leads to a roughly 2:1 ratio of ortho and para nitration.

IV. Mechanistic Relevance of Charge-Transfer Nitration to the Electrophilic Nitration of Various Aromatic Donors. Thermal (electrophilic) and photochemical (charge-transfer) nitrations share in common the rapid, preequilibrium formation of the EDA complex [ArH , $PyNO_2^+$] in eq 1. Therefore let us consider how charge-transfer activation, as established by the kinetic behavior of the reactive triad in Scheme III, relates to a common mechanism for electrophilic nitration. Since the reactive intermediates pertinent to the thermal (electrophilic) process, unlike those in its photochemical counterpart, cannot be observed directly, we must rely initially on the unusual array of (nonconventional) nitration products^{20,21} and the unique isomeric distributions as follows.

A. Isomeric product distributions obtained from toluene and anisole have been the subject of considerable mechanistic discussion in electrophilic aromatic nitration.⁷⁷ As applied to nitrations with *N*-nitropyridinium, the yellow color of the EDA complex immediately attendant upon the mixing of toluene and $PyNO_2^+$ in acetonitrile persists for about a day (in the dark), whereas the charge-transfer color of toluene and $Me_2PyNO_2^+$ is discharged within 10 min at 25 °C. Both bleached solutions afford an identical mixture, i.e.



o- (62%), *m*- (4%) and *p*-nitrotoluenes (34%)¹⁶ that also obtains from the electrophilic aromatic nitration of toluene with more conventional nitrating agents such as nitric acid, acetyl nitrate, etc.⁷⁷ Most importantly, the isomeric composition derived in eq 34 from the electrophilic nitration of toluene is experimentally indistinguishable from that produced in charge-transfer nitration according to Scheme VII. Such an identity is not a coincidence, since the electrophilic nitration of anisole (Table II, entry 2) affords an isomeric mixture of *o/p*-nitroanisole that is the same as that obtained from charge-transfer nitration in Scheme VIII.

(74) The promotion of the homolytic pathway by added NO_2 is not feasible for anisole, owing to the rapid thermal reaction. See: Underwood, G. R.; Silverman, R. S.; Vandervelde, A. *J. Chem. Soc., Perkin Trans. 2*, **1973**, 1177. Radner, F.; Wall, A.; Loncar, M. *Acta Chem. Scand.* **1990**, *44*, 152.

(75) (a) O'Neill, P.; Steenken, S.; Schulte-Frohlinde, D. *J. Phys. Chem.* **1975**, *79*, 2773. (b) Bachler, V.; Steenken, S.; Schulte-Frohlinde, D. *J. Phys. Chem.* **1991**, *95*, 6811. See, also: Feng, J.; Zheng, X.; Zerner, M. C. *J. Org. Chem.* **1986**, *51*, 4531.

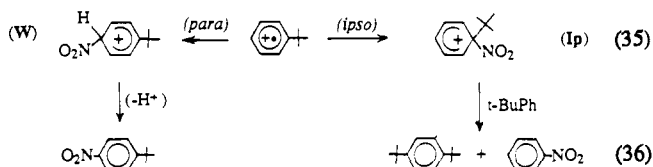
(76) However, we hasten to add that the charge density on the aromatic cation radical may not be the sole (or even principal) factor that determines the isomeric product distribution. Thus the extent to which either the homolytic or nucleophilic addition, or both, is reversible relative to the rate of the follow-up process [i.e., deprotonation in eqs 28/32 and NO_2 coupling in eqs 29/33, respectively] will determine the relative (overall) contribution from these competing pathways. For the kinetics of this mechanistic situation, see: (a) Sykes, P. *The Search for Organic Reaction Pathways*; Longman: London, 1972, p 33f. (b) Noyes, R. M. In *Investigation of Rates and Mechanisms of Chemical Reactions, Part I*; Bernasconi, C. F., Ed.; Wiley: New York, 1986; p 410f.

(77) For a summary, see: Olah et al. in ref 2, pp 150–2 for toluene nitration. Schofield, K. in ref 1, pp 241–4 for anisole nitration.

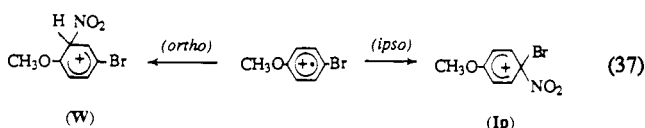
Moreover, the same conclusion extends to the regiochemical changeover to preferential para (and significant meta) nitration of the sterically hindered *tert*-butylbenzene that is effected in the dark (electrophilic)¹⁶ as well as with light (charge-transfer) in Table V, entry 1. Therefore we conclude that the activation processes leading to the electrophilic nitration of toluene, anisole, and *tert*-butylbenzene cannot be distinguished from those in Schemes VII and VIII on the basis of the isomeric distributions of nitrotoluenes, nitroanisoles, and nitro-*tert*-butylbenzenes.

B. Nuclear and side-chain nitration are diagnostic of the kinetic competition in polymethylbenzene reactivity.^{20,21} As such, the direct parallel between electrophilic and charge-transfer nitrations is revealed in ring and side-chain nitration, especially of durene and pentamethylbenzene. For example, the relative amounts of nitrodurene (**R**) and α -nitrodurene (**SC**), obtained in charge-transfer nitration with the various X-substituted *N*-nitropyridinium in Table IV, are essentially identical to those previously obtained in the electrophilic nitration of durene.¹⁶ Moreover, the relative contribution from the third pathway leading to the oxidative dimer (**D**) is the same for electrophilic¹⁶ and charge-transfer nitration (column 6, Table IV). The same parallel also applies to the ring/side-chain nitration and the oxidative dimerization of pentamethylbenzene under electrophilic¹⁶ and charge-transfer conditions (Table IV, entries 7 and 8). We thus conclude that the competition between homolytic addition and deprotonation of the aromatic cation radical as described in Scheme VI also adequately describes the activation process for electrophilic nitration.

C. Ipso adduct as a reactive intermediate in aromatic substitution is diagnostic of the electrophilic reactivity of the nitrating agent, particularly toward the following prototypical aromatic donors.^{1,2} ***tert*-Butylbenzene**. The competition for para and ipso attack leads to the Wheland intermediate (**W**) and ipso adduct (**Ip**) in eq 35, i.e.

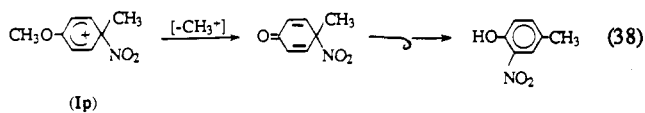


that are responsible for the simultaneous nitration and *trans*-alkylation of *tert*-butylbenzene leading to 4-*tert*-butylnitrobenzene and di-*tert*-butylbenzene (nitrobenzene), respectively, as given in eq 36.^{29,78} It is thus noteworthy that the dual pathways in eq 35 as well as the isomeric product distributions in the charge-transfer nitration of *tert*-butylbenzene (Table V, entry 1) are the same as those previously observed in electrophilic nitration.¹⁶ **Bromoanisole**. The competition between ortho and ipso attack, i.e.

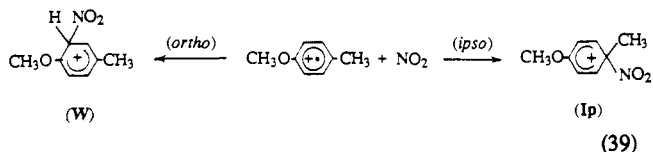


is also pertinent to the simultaneous nitration and *trans*bromination of 4-bromoanisole according to eq 8.⁷⁹ Charge-transfer nitration leads to mixture of 2-nitro-4-bromoanisole and 2,4-dibromoanisole (4-nitroanisole) in Table V, the relative amounts of which are equivalent to those obtained in the electrophilic nitration of 4-bromoanisole (see Experimental Section). **Methylanisole**. The competition between ortho and ipso attack (analogous to that depicted in eq 37) applies to the simultaneous nitration and *demethylation* of 4-methylanisole according to eq 9. The identification of 4-nitro-4-methylcyclohexa-2,5-dienone

as the metastable intermediate in Table V is particularly diagnostic of the ipso adduct, i.e.

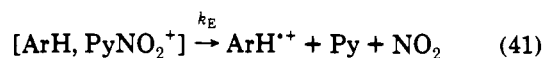


that is also apparent in the electrophilic nitration of 4-methylanisole.¹³ The common bifurcation of nitration pathways resulting from para(ortho) and ipso attack on the various aromatic donors, as noted above, indicates that the activation step leading to the Wheland intermediate (**W**) and the ipso adduct (**Ip**) in electrophilic nitration is indistinguishable from that in charge-transfer nitration. Since time-resolved spectroscopy establishes the latter as the homolytic annihilation of the aromatic cation radical by NO₂, we conclude that the same (or a very closely related) ion radical pair is involved in electrophilic aromatic substitution.



In view of the striking similarities that are consistently delineated in all three aspects dealing with (a) the isomeric product distributions, (b) nuclear versus side-chain nitration, and (c) ipso adducts, the most direct formulation of electrophilic nitration invokes the production of the same intermediates (as those in the reactive triad in Scheme I) via a purely thermal process, e.g.

Scheme IX



Since electron transfer ($\log k_{\text{E}}$) represents the adiabatic counterpart to the photochemical process ($h\nu_{\text{CT}}$), the triad in eq 41 is (stoichiometrically) equivalent to that in eq 15; and its collapse to the Wheland intermediate would lead to nitration products that are the same as those formed in charge-transfer nitration. When such a comparison of electrophilic and charge-transfer nitrations is carried out in quantitative detail, the aromatic donors fall roughly into two categories: (1) *Reactive arenes* including the electron-rich anthracenes and naphthalenes^{14,17} as well as hexamethylbenzene, pentamethylbenzene, durene, and various 4-substituted anisoles¹³ show reactivity patterns in (a), (b) and (c) that are singularly indistinguishable for electrophilic and charge-transfer nitrations—more or less independent of the particular nitrating agent employed. (2) *Less reactive arenes* such as anisole, toluene, *tert*-butylbenzene, and mesitylene also show the same reactivity patterns in (a) and (c), but only when the electrophilic and charge transfer nitrations are carried out with either the sterically hindered Me₂PyNO₂⁺ or MeOPyNO₂⁺ in the presence of added NO₂. Since the latter conditions pertain to aromatic nitration solely via the homolytic annihilation of the cation radical (see ArH^{•+} in Scheme VII), it follows from the isomeric distributions in eq 34 that the electrophilic nitrations of the less reactive aromatic donors (toluene, mesitylene, anisole, etc.) also proceed via Scheme IX. If so, why do the electrophilic and charge-transfer pathways diverge when the less reactive aromatic donors are treated with other *N*-nitropyridinium reagents, particularly those derived from the electron-rich MeOPy and MePy? The conundrum is cleanly resolved in Figure 6,⁸⁰

(78) (a) Schofield in ref 1, p 199ff. (b) Legge, D. I. J. Am. Chem. Soc. 1947, 69, 2086.

(79) Perrin, C. L. J. Org. Chem. 1971, 36, 420.

(80) The rate data in Figure 6 are taken from Table X and refs 27, 64, and 71, and the values of E_{ox} from refs 13, 32a, and 64.

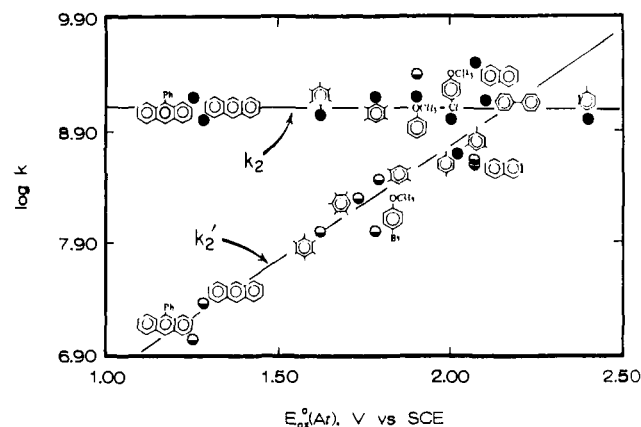
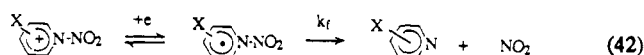


Figure 6. Variation of the rate constants for the homolytic (k_2) and nucleophilic (k_2') annihilation of various aromatic cation radicals with NO_2 and pyridine, respectively, as a function of the oxidation potential E_{ox}^0 (to gauge $\text{ArH}^{+\bullet}$ stability⁵¹).

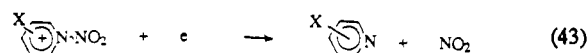
which shows the rate of homolytic annihilation of aromatic cation radicals by NO_2 (k_2) to be singularly insensitive to cation-radical stability, as evaluated by E_{ox}^0 .⁵¹ By contrast, the rate of nucleophilic annihilation by pyridine (k_2') shows a distinctive downward trend that decreases monotonically from toluene cation radical to anthracene cation radical. Indeed, the divergent curves in Figure 6 predict the significant domination of the homolytic pathway (k_2) for reactive (class 1) arenes. Consequently, nucleophilic annihilation (k_2') is unimportant for durene, 4-bromoanisole, and pentamethylbenzene, and a common mechanism based on homolytic annihilation (k_2) is mutually shared in the electrophilic and charge-transfer nitrations of these electron-rich aromatic donors. On the other hand, the curve crossing observed in the region about $E_{\text{ox}}^0 = 2.2$ V for mesitylene, toluene, and anisole predicts that homolytic and nucleophilic pathways are competitive ($k_2 \sim k_2'$) for the triad from less reactive (class 2) arenes. This also explains why the competition is dependent on the pyridine nucleophile—being most pronounced with MeOPy [as indicated by the actual trapping of $\text{MES}^{+\bullet}$, the increase in meta nitration from $\text{TOL}^{+\bullet}$ and the dominance of para nitration from $\text{AN}^{+\bullet}$ in eqs 24, 29, and 33, respectively] and essentially nil with Me_2Py [as indicated by the absence of $\text{MES}^{+\bullet}$ trapping and the normal isomeric patterns from $\text{TOL}^{+\bullet}$ and $\text{AN}^{+\bullet}$ in Tables IV, III, and II, respectively].

Finally we ask, if the reactive triads in Schemes I and IX are common to both electrophilic and charge-transfer nitration, why is the nucleophilic pathway (k_2') apparently not pertinent to the electrophilic activation of toluene and anisole? One obvious answer is that the electrophilic nitration of these less reactive (class 2) arenes proceeds via a different mechanism, in which NO_2 is directly transferred from *N*-nitropyridinium in a single step, without the intermediacy of the reactive triad, since such an activation process relates to the more conventional view of electrophilic aromatic substitution.⁷⁷ However, the concerted mechanism for toluene, anisole, mesitylene, *tert*-butylbenzene, etc. does not readily accommodate the three unique facets that relate charge transfer directly to electrophilic nitration in this study, viz., the lutidine syndrome, the added NO_2 effect, and the TFA neutralization (of Py). Accordingly, let us return to Schemes I and IX and inquire into the nature of thermal (adiabatic) electron transfer in eq 41 vis à vis the (vertical) charge transfer in eq 14. [At this juncture, time-resolved spectroscopy is unable to provide the requisite mechanistic guide, since the kinetics of the Wheland intermediate (**W**) and the nucleophilic adduct (**N**) cannot be observed simultaneously.^{63b,c]}

Triad formation in Scheme I is a two-step process involving the metastable *N*-nitropyridinyl radical, i.e.⁵⁵



whereas the adiabatic electron transfer in Scheme IX is likely to occur irreversibly with the simultaneous cleavage of the $\text{N}-\text{NO}_2$ bond, i.e.,



As a result the nascent pair (Py and NO_2) in eq 42 can suffer greater diffusive separation from $\text{ArH}^{+\bullet}$ compared to that in eq 43. If so, the complexation of the aromatic cation radical by pyridine, i.e.



as recently delineated by Reitstøen and Parker⁶⁴ is (kinetically) expected to play a more important role in the thermal compared to the photochemical process. The sequestering of pyridine in this manner will lead to its decreased nucleophilic reactivity, especially toward aromatic cation radicals derived from the less reactive (class 2) donors. Thus, if the rate processes in eqs 42–44 occur on the time scale competitive with the homolytic annihilation of the aromatic cation radical by NO_2 in Table VII, they could form the basis for the mechanistic distinction of the reactive triads in Schemes I and IX. [Complex formation is not expected to affect the regiochemistry, since the aromatic cation radical as a planar moiety will be subject to the same steric access by NO_2 irrespective of whether it is shielded on one face⁸¹—the loose pyridine association extant in $[\text{ArH}^{+\bullet}, \text{Py}]$ being insufficient to differentiate the Wheland intermediates from those derived directly from $\text{ArH}^{+\bullet}$.^{17]}

The electron-transfer mechanism for electrophilic aromatic nitration as presented in Scheme IX is consistent with the CIDNP observation in related systems,^{82a} in which the lifetime of the radical pair (cf. eq 41) is of particular concern.^{82b,83} As such, other types of experimental evidence for aromatic cation radicals as intermediates in electrophilic aromatic nitration are to be found only when there is significant competition from (dissociative) rate processes on the time scale of $\tau < 10^{-10}$ s.⁸⁴ Under these general circumstances, it is important to emphasize that an endergonic driving force for electron transfer, as evaluated from the values of E_{ox}^0 of $\text{ArH}^{+\bullet}$ and E_{red}^0 of NO_2Y^{55} , does not necessarily present a kinetics restriction on the electrophilic (thermal) process for anisole, toluene, or even benzene.⁸⁵

Summary and Conclusions

N-Nitropyridinium (XPyNO_2^+) is a uniquely versatile reagent for both the electrophilic (thermal) and charge-transfer (photochemical) nitration of various aromatic donors (ArH), in which the *X*-substituent modulates (a) the reactivity of XPyNO_2^+ , both with respect to electron demand as well as steric crowding, and

(81) For the role and properties of related complexes of $\text{ArH}^{+\bullet}$, see: Kim et al. in ref 17. Badger, B.; Brocklehurst, B. *Trans. Faraday Soc.* **1969**, 2576, 2588.

(82) (a) Clemens, A. H.; Ridd, J. H.; Sandall, J. P. B. *J. Chem. Soc., Perkin Trans. 2* **1984**, 1659; **1985**, 1227. Johnston, J. F.; Ridd, J. H.; Sandall, J. P. B. *J. Chem. Soc., Perkin Trans. 2* **1991**, 623. (b) Note the absence of CIDNP with mesitylene does not preclude the existence of (geminate) radical pairs, since the requisite cage escape of the reactive $\text{MES}^{+\bullet}$ may be too slow for development of nuclear polarization (see: Kaptein, R. *Adv. Free-Radical Chem.* **1975**, 5, 319.

(83) For recent summaries of electron-transfer mechanism in electrophilic aromatic nitration, see: Morkovnik, A. S. *Russ. Chem. Rev.* **1988**, 57, 144. Ridd, J. in ref 59. Olah, G. et al. in ref 2. See, also: Rudakov, E. S.; Lobachev, V. L. *Dokl. Akad. Nauk SSR (Engl. Trans.)* **1991**, 314, 286. Keumi, T.; Hamanaka, K.; Hasegawa, H.; Minamide, N.; Inoue, Y.; Kitajima, H. *Chem. Lett.* **1988**, 1285.

(84) For example, the characteristic C—C bond scission of labile cation radicals has been observed only during the electrophilic nitration of aromatic donors such as the dianthracenes and bicumene analogues¹⁶ which produce $\text{ArH}^{+\bullet}$ with fragmentation rates of $k_f > 10^{10}$ s⁻¹.

(85) See: (a) Perrin, C. L. *J. Phys. Chem.* **1984**, 88, 3611. (b) Bertran, J.; Gallardo, I.; Moreno, M.; Savéant, J. M. *J. Am. Chem. Soc.* **1992**, 114, 9576. See, also: Lee, K. Y.; Amatore, C.; Kochi, J. K. *J. Phys. Chem.* **1991**, 95, 2285. Kochi, J. K. in ref 18. The dichotomy may also be expressed in terms of a concerted or a two-step process, as in the $\text{S}_{\text{N}}2$ transition state: Shaik, S. S. *Pure Appl. Chem.* **1991**, 63, 195.

(b) the nucleophilic strength of the pyridine base (XPy) generated in situ. Thus the nitrating agent from 2,6-lutidine ($\text{Me}_2\text{PyNO}_2^+$) produces the sterically hindered base (Me_2Py) which is an ineffective nucleophile, whereas that from 4-methoxypyridine (MeOPyNO_2^+) leads to the strong base MeOPy which is also a powerful nucleophile. Indeed, such a highly contrasting behavior of $\text{Me}_2\text{PyNO}_2^+$ and MeOPyNO_2^+ provides an invaluable mechanistic tool for the detailed probing of the reactive intermediates which are directly observable in charge-transfer nitration.

Time-resolved spectroscopy unambiguously establishes ArH^{++} , XPy, and NO_2 as the reactive triad in Scheme I for the charge-transfer activation of aromatic EDA complexes with *N*-nitropyridinium. When the nitrating agent is the sterically hindered $\text{Me}_2\text{PyNO}_2^+$, homolytic annihilation of ArH^{++} with NO_2 defines the critical Wheland intermediate (W) in the charge-transfer nitration of various aromatic donors (compare Scheme II). As such, the nitration products from toluene, anisole, and *tert*-butylbenzene as well as different polymethylbenzenes and substituted anisoles [all specifically selected for the characteristic isomeric distributions and multiple (nonconventional) products] are found to be *singularly indistinguishable* from those obtained via the corresponding electrophilic (thermal) process. When the nitrating agent is MeOPyNO_2^+ , the same identity also pertains to electrophilic and charge-transfer nitrations—*provided* the competition from the extraneous nucleophilic annihilation of ArH^{++} with MeOPy via the nucleophilic adduct (N in Scheme V, eqs 29 and 33) is specifically and quantitatively taken into account in the photochemical process.

Since electrophilic and charge-transfer nitrations are both initiated via the same EDA complex (see eq 2) and finally lead to the same array of nitration products, we infer that they share the intermediate stages in common. The strength of this inference rests on the variety of aromatic substrates (with widely differing reactivities and distinctive products) to establish the mechanistic criteria by which the identity of the two pathways are exhaustively tested. On this basis, we conclude the electrophilic nitration is operationally equivalent to charge-transfer nitration in which electron-transfer activation is the obligatory first step. The extent to which the reactive triad in eq 44 is subject to intermolecular interactions in the first interval (few picoseconds) following electron transfer will hopefully further define the mechanistic nuances of dissociative electron transfer in adiabatic and vertical systems.

Experimental Section

The aromatic donors and various *N*-nitropyridinium salts ($\text{XPyNO}_2^+\text{BF}_4^-$) used in this study were as described previously.¹⁶ Spectral (UV-vis, IR, ^1H and ^{13}C NMR) analyses, together with product identification and quantification, generally followed along the previous studies on electrophilic nitration.^{16,17} **General Procedure for Charge-Transfer Nitration.** Typically 4×10^{-5} mol of 4-X-PyNO₂⁺BF₄⁻ was placed in a 10-mm square quartz cuvette equipped with side arm and Schlenk adapter. The cell was taken out of the drybox and connected to a vacuum line, and 1 mL of acetonitrile was added with the aid of a hypodermic syringe. An aliquot of 0.04 M arene in acetonitrile (1 mL) was carefully cannulated into the side arm of the UV cell. The cuvette was thermally equilibrated in the low-temperature bath contained in a transparent Pyrex dewar and maintained at 0 – -60 ± 2 °C with a Neslab CC-65A refrigerated thermoregulator. The duplicate, dark control was always carried out simultaneously in a light-tight cuvette to monitor any thermal process. The light source for charge-transfer nitration consisted of a 500 W Osram HB mercury lamp equipped with a parabolic reflector.

The light was passed through a circulating water filter to remove IR radiation, and a fused silica biconvex lens (ϕ 4.5 cm, *f* 10 cm) focussed the light onto the sample contained in 1.0-cm quartz cuvette. Either a sharp cutoff filter (Corning CS-3 series) or a broad band filter (350–580 nm, Corning 4309) was fixed in front of the cell to ensure that only the charge-transfer band of the relevant EDA complex was irradiated. After mixing, the yellow to orange solution was irradiated continuously and the progress of the photolysis was periodically monitored by changes in the UV-vis and ^1H NMR spectra of the photolysate. Finally, diethyl ether and water were added, and the ethereal extract was subject to quantitative GC and/or HPLC analysis by the internal standard method. For the detailed workup and analytical procedures for each of the arenes in Tables II–V, see supplementary material.

Time-Resolved Spectroscopy and the Spectral Decays of Aromatic Cation Radicals. The time-resolved differential absorption spectra on the picosecond time scale (Table VI) were obtained with a laser-flash system that utilized the 532 (second harmonic) and 355 nm (third harmonic) 20-ps pulses from a Quantel YG501-C mode-locked Nd:YAG laser as the excitation sources. The excitation beam was focused onto the sample with a cylindrical (fused silica) lens (*f*₂), as described previously.⁵⁵ The time-resolved spectral studies on the nanosecond/microsecond time scales were carried out with a spectrometer consisting of Quantel YG580-10 Q-switched Nd:YAG laser with a pulsewidth of 10 ns. The probe beam, consisting of the output from a 150 W xenon arc lamp mounted in an Oriel housing that was equipped with an Aspherlab UV-grade condensing lens, was focussed onto the sample, and the emerging beam from the sample was focussed onto the entrance slit of an Oriel 77250 monochromator.¹³ The spectral decays were collected from 10–40 traces and averaged to obtain the data for each kinetics determination (see for example, Figure 4B). The observed ns/ μs absorbance changes at λ_{mon} for the arenes cation radicals were fitted to first- or second-order decays using ASYST 2.0 software (Tables IX and X). In order to test the validity of the second-order kinetics decays, the laser irradiation energy was varied and the second-order rate constants and half-lives were determined as a function of the initial absorbance A_0 (Table VIII). The quantum yield for arene cation radical production in Table VII is given by $\Phi = (A/A_{\text{BP}}) (7220/\epsilon)$ where ϵ is the extinction coefficient of the arene cation radical and the value of ϵ_{BP} was taken as $7220 \text{ M}^{-1} \text{ cm}^{-1}$ according to Hurley et al.⁴⁶ The ratio A/A_{BP} did not vary upon changing the laser power between 5.0 and 30 mJ per shot. The extinction coefficients of the polymethylbenzene cation radicals were obtained from the pulse-radiolysis studies of Sehested et al.⁴³ For anisole and the substituted anisoles, these values were obtained by quenching of the arene triplet with methylviologen (MV^{2+}). Benzophenone (6×10^{-3} M in MeCN) was excited at 355 nm in the presence of anisole (0.1 M) and methylviologen [0.05 M as the bis(trifluoromethanesulfonate) salt] and the absorbance of the cation radical (A at λ_{max}) was compared with the 610-nm absorbance of MV^+ . Residual (minor) absorptions corresponding to the spectra of the nucleophilic adducts⁴⁴ to various ArH^{++} are described in the supplementary material together with other spectral details.

Acknowledgment. We thank the National Science Foundation, the Robert A. Welch Foundation, and the Texas Advanced Research Project for financial support.

Supplementary Material Available: The materials and instrumentation used, the charge-transfer nitration of anisole, toluene, durene, pentamethylbenzene, *p*-xylene, mesitylene, hexamethylbenzene, *tert*-butylbenzene, 4-bromoanisole, 4-methylanisole, bromobenzene, and the electrophile nitration of 4-bromoanisole and *p*-xylene are described in detail, together with the time-resolved (picosecond and nanosecond/microsecond) spectroscopy, the spectral decay kinetics, the isotope effects, and the quantum efficiencies for the production of aromatic radicals (26 pages). Ordering information is given on any current masthead page.